

# A microRNA-mRNA expression network during oral siphon regeneration in *Ciona*

Elijah J. Spina<sup>1</sup>, Elmer Guzman<sup>1</sup>, Hongjun Zhou<sup>2</sup>, Kenneth S. Kosik<sup>1,2</sup> and William C. Smith<sup>1,2,\*</sup>

## ABSTRACT

Here we present a parallel study of mRNA and microRNA expression during oral siphon (OS) regeneration in *Ciona robusta*, and the derived network of their interactions. In the process of identifying 248 mRNAs and 15 microRNAs as differentially expressed, we also identified 57 novel microRNAs, several of which are among the most highly differentially expressed. Analysis of functional categories identified enriched transcripts related to stress responses and apoptosis at the wound healing stage, signaling pathways including Wnt and TGF $\beta$  during early regrowth, and negative regulation of extracellular proteases in late stage regeneration. Consistent with the expression results, we found that inhibition of TGF $\beta$  signaling blocked OS regeneration. A correlation network was subsequently inferred for all predicted microRNA-mRNA target pairs expressed during regeneration. Network-based clustering associated transcripts into 22 non-overlapping groups, the functional analysis of which showed enrichment of stress response, signaling pathway and extracellular protease categories that could be related to specific microRNAs. Predicted targets of the *miR-9* cluster suggest a role in regulating differentiation and the proliferative state of neural progenitors through regulation of the cytoskeleton and cell cycle.

**KEY WORDS:** Regeneration, RNAseq, MicroRNA, *Ciona*, Correlation network

## INTRODUCTION

The ability of metazoan animals to regenerate varies widely. This ability can be interpreted as a spectrum extending from extreme cases of whole-body regeneration, such as is observed in planaria (Reddien and Sánchez Alvarado, 2004), to cases of limited cell replacement during tissue homeostasis, such as is observed in the mammalian digestive tract (Barker, 2014; Barker et al., 2008). In addition, many species display regenerative capacities that vary with life stage and injury severity (Rinkevich and Rinkevich, 2012). Most vertebrates, including humans, heal wounds using fibrotic mechanisms that inhibit subsequent tissue regrowth by leaving dense connective tissue that is never remodeled to the original functional state (Harty et al., 2003). By contrast, there are several well-characterized examples of vertebrates that are able to replace whole organs and/or appendages composed of multiple tissue types (King and Newmark, 2012; Stoick-Cooper et al., 2007). Furthermore, differences in cellular responses appear to directly

underlie the differences in regenerative capacity of various organisms, as evidenced by differences in scar formation between regenerating vertebrates (e.g. salamanders) and non-regenerating vertebrates (Seifert et al., 2012). Regeneration is likely to be an ancestral animal trait that utilizes many of the molecular mechanisms of development, thus implying evolutionary loss of this trait in some lineages (Bely and Nyberg, 2010; Morgan, 1901; Tiozzo and Copley, 2015). By identifying points of evolutionary conservation and divergence in the molecular mechanisms underlying regeneration, progress can be made toward illuminating how different species can accomplish the same task in vastly different ways.

Whereas regenerative ability is highly variable among the vertebrates, and whole-organ regeneration is limited to very few species, the tunicates, which are primitive chordates and the closest extant relatives of the vertebrates (Delsuc et al., 2006), show robust regenerative ability. Tunicates appear to have diverged before two whole-genome duplications that are speculated to have occurred at the origin of the vertebrate lineage (Dehal and Boore, 2005), and are thought to have subsequently evolved towards reduced morphological and genomic complexity (Crow and Wagner, 2006). These traits, in combination with a sequenced and well-annotated genome, make *C. robusta* a powerful model for identifying the components and interactions that comprise gene regulatory networks that govern biological processes, including regeneration (Dehal et al., 2002; Satou et al., 2008). The colonial tunicates, such as *Botryllus schlosseri*, show whole-body regeneration (Kürn et al., 2011; Rinkevich et al., 1995, 2010; Voskoboynik et al., 2007). *Ciona intestinalis* and *Ciona robusta*, two species that until recently were both called *Ciona intestinalis* (Brunetti et al., 2015), are well-established models for embryology, and as adults they can rapidly and robustly regenerate their oral siphons as well as their central nervous systems (Jeffery, 2015a). The oral siphon (OS) is a cylindrical appendage composed primarily of muscular tissue, vasculature, nerves, epidermis, eight oral pigment organs (OPOs) located at the distal tip, and an outer coating of tunic (Chiba et al., 2004).

Although many studies have identified molecular mechanisms governing cellular responses during regeneration, little is known about how different molecular events are coordinated with each other (Endo et al., 2004; Jhamb et al., 2011; King and Newmark, 2012). This deficiency is evident in the current lack of effective molecular therapies available to stimulate tissue regeneration (Stoick-Cooper et al., 2007). The ability to detect transcript level changes in a comprehensive and unbiased manner can identify previously unknown coordination between signaling pathways, transcription factors and effector genes required for regeneration. There have been several transcriptome-wide studies of gene expression of both mRNA (Campbell et al., 2011; Hamada et al., 2015; Knapp et al., 2013; Love et al., 2011; Monaghan et al., 2009; Schebesta et al., 2006; Stewart et al., 2013; Wu et al., 2013) and

<sup>1</sup>Department of Molecular, Cell and Developmental Biology, University of California, Santa Barbara, Santa Barbara, CA 93106, USA. <sup>2</sup>Neuroscience Research Institute, University of California, Santa Barbara, Santa Barbara, CA 93106, USA.

\*Author for correspondence (william.smith@lifesci.ucsb.edu)

© W.C.S., 0000-0002-6257-7695

microRNA (miRNA) (Gearhart et al., 2015; Holman et al., 2012; Hutchins et al., 2016; Thatcher et al., 2008) during appendage regeneration. However, none of these studies connected the expression profiles of miRNA to those of mRNA.

In the current study, we present a transcriptome-wide investigation of both mRNA and miRNA expression profiles from stage-matched samples during appendage regeneration of *C. robusta*. We constructed a network of correlations between these two RNA types and inferred the function of miRNAs within a network based on the functions of their predicted target mRNAs. Our approach expands upon previous work by analyzing tissues both distal and proximal to the amputation plane using high-throughput RNA sequencing (RNAseq) of miRNAs and mRNAs, then comparing relative expression levels between distinct stages of regeneration. We identified the largest changes in gene expression during OS regeneration and conducted a systematic characterization of functional categories of all genes as well as those predicted to be targeted by specific miRNAs. This study provides a resource that will facilitate future investigation into the genetic requirements of appendage regeneration in chordates. To make our results comparable with those of a previous microarray study (Hamada et al., 2015) we also sequenced RNA from non-regenerating OSs and identified several of the same genes that they identified as the most significantly differentially expressed at 3 days post-amputation.

## RESULTS

### Differential expression during OS regeneration

High-throughput RNAseq was used to estimate the relative abundance of mRNAs and miRNAs in OSs of 6-month-old *C. robusta* adults. As an initial validation of our approach, mRNA samples were collected from non-regenerating (NR) OSs and used to estimate the efficiency of read alignment and power to detect differentially expressed (DE) genes based on sequencing depth and number of replicates. In this preliminary analysis, we successfully aligned an average of 92.6% (94.8% across all stages) of sequencing reads to *C. robusta*, with ~63.6% (58.4% across all stages) of reads aligning to unique genomic locations (Table S1). Next, we estimated the power of our chosen experimental design to accurately quantify differential expression using the Scotty web tool (Busby et al., 2013). Given the sequencing depth and variation within the NR OS samples, we could expect to recover nearly half of the genes that are DE greater than 2-fold at any stage as significantly DE [false discovery rate (FDR)  $\leq 0.05$ ] using our experimental design (Fig. S1).

For collection of regenerating tissue samples, animals were amputated distal to the buccal tentacle band (Chiba et al., 2004) (Fig. 1). Either immediately following amputation [day (D) 0] or 1, 3 or 8 days following amputation (D1, D3 or D8) tissue was collected by making a second cut proximal to the first, but distal to the peripharyngeal (transverse) muscle band (Fig. 1, yellow dashed lines). These time points were chosen to represent three stages of regeneration observed in vertebrates: wound healing, transition and redevelopment. Previous reports of differential expression had used NR OSs for comparison (Hamada et al., 2015). It was expected that comparisons of subsequent stages with either D0 or NR OSs would generate different categories as being enriched, and that by using both a fuller picture would be generated. Three biological replicate cDNA libraries of each type (miRNA and mRNA) were prepared from the D0, D1, D3 and D8 tissue samples. In total, 12,700 of the 17,745 *C. robusta* mRNA transcript models were detected in the mRNA library sequence reads using a threshold of  $\geq 5$  RPKM (reads

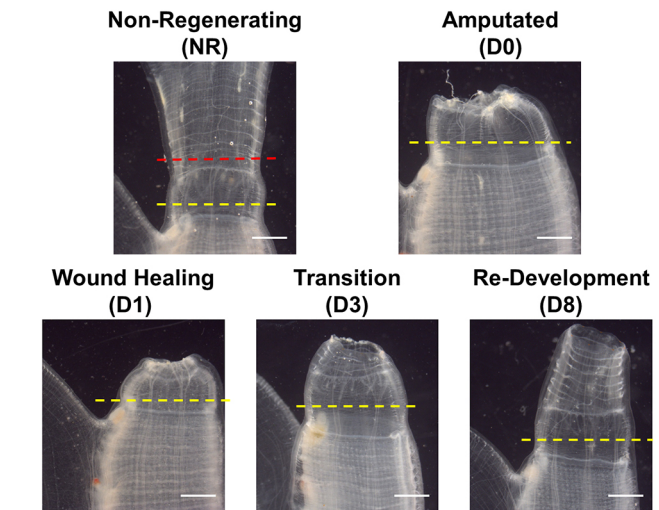


**Fig. 1. Stages of oral siphon regeneration.** (Top) The two reference stages used to quantify relative expression levels at subsequent stages. Left image shows an unamputated adult oral siphon (OS) of *C. robusta*; the right image is immediately post-amputation. (Bottom) Three time points (1, 3 and 8 D) selected to represent three stages of appendage regeneration (wound healing, transition and redevelopment, respectively). The red dashed line indicates the original amputation plane, and the yellow dashed lines indicate the proximal limit of tissue collected for expression profiling. Scale bars: 5 mm.

per kilobase of transcript per million mapped reads) in three or more samples.

Analysis was performed using two programs in parallel: EdgeR (Robinson et al., 2010) and DESeq2 (Love et al., 2014a). Only transcripts identified as DE by both programs were used in order to reduce the likelihood of false positives, as has been described previously (Robles et al., 2012). The EdgeR and DESeq2 programs identified 337 and 472 of the mRNA transcript models, respectively, to be DE (FDR  $\leq 0.05$ ) on at least one of the days of regeneration (i.e. D1, D3 or D8) when compared with D0. Of the DE genes on these two lists, 248 overlapped (Table S2). A roughly equivalent number of mRNAs were upregulated or downregulated (Table 1). We assessed the expression of 15 DE mRNA transcripts using quantitative real-time PCR (qRT-PCR), with particular attention to transcripts linked to morphogenetic processes and signaling pathways (Fig. 2A). Of these, nine were validated using qRT-PCR in at least one stage during regeneration (Fig. 2A). For example, transcripts for the tumor necrosis factor receptor (TNFr) and an auxiliary protein (TNFr-associated) were found to be significantly ( $P \leq 0.05$ ) downregulated by both RNAseq and qRT-

**Table 1. Number of DE transcripts at post-amputation stages relative to D0**

| Sample type | Method      | LRT | D1 (+/-) | D3 (+/-) | D8 (+/-) |
|-------------|-------------|-----|----------|----------|----------|
| miRNA       | EdgeR       | 15  | 4/11     | 4/11     | 6/9      |
|             | DESeq2      | 23  | 8/15     | 7/16     | 8/15     |
|             | Concurrence | 14  | 4/10     | 4/10     | 5/9      |
| mRNA        | EdgeR       | 337 | 178/159  | 204/133  | 186/151  |
|             | DESeq2      | 472 | 244/228  | 254/218  | 252/220  |
|             | Concurrence | 248 | 132/116  | 150/98   | 138/110  |

Transcripts included in pairwise comparisons (D1, D3 or D8 versus D0) were selected using likelihood ratio tests (LRT) (FDR  $\leq 0.05$ ) by either EdgeR, DESeq2 or the concurrence of both programs. The total number of DE transcripts across all comparisons determined by LRT is indicated as well as the number of transcripts upregulated/downregulated (+/-) for each pairwise comparison.

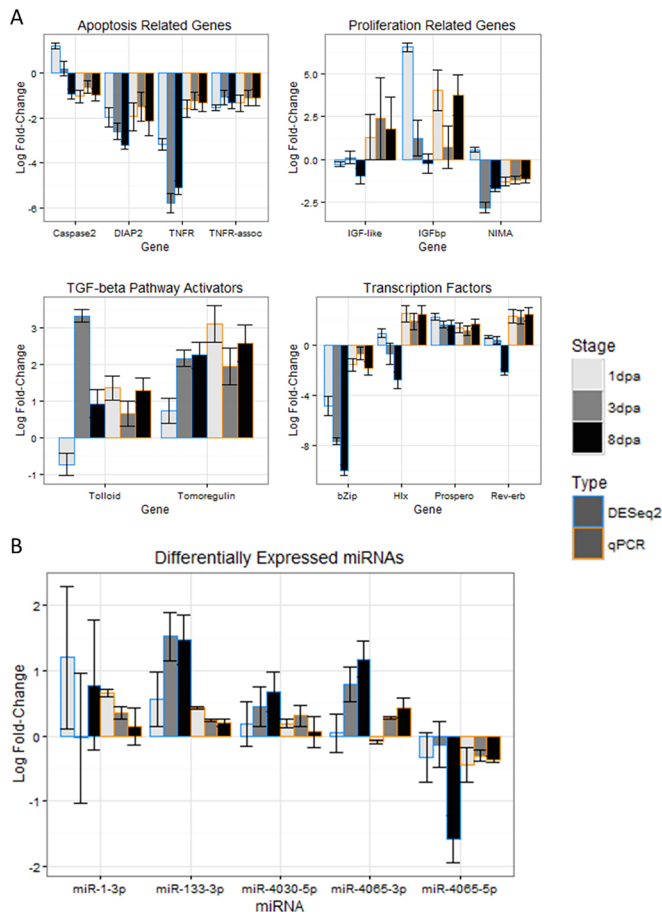


**Fig. 2. Experimental validation of differential expression.** The mean  $\log_2$  fold change of transcript expression levels relative to D0 estimated by RNAseq (DESeq2) and qRT-PCR. Three biological replicates comprising three technical replicates each were used to calculate qRT-PCR statistics; error bars indicate s.e.m. for RNAseq and 95% confidence intervals for qRT-PCR. (A) Differentially expressed (DE) mRNAs significant in both RNAseq and qRT-PCR experiments arranged into preselected groups. Ensembl transcript identifiers matching each transcript name are listed in Table S8. (B) DE miRNAs significant in both RNAseq and qRT-PCR data.

PCR at all stages post-amputation (Fig. 2A). We also confirmed that the expression of two potential activators of transforming growth factor  $\beta$  (TGF $\beta$ ) signaling were significantly upregulated during regeneration (Fig. 2A). These two pathways have previously been implicated in the regulation of programmed cell death and proliferation during regeneration (Gilbert et al., 2013; Godwin et al., 2013; Ho and Whitman, 2008; Lévesque et al., 2007; Rao et al., 2009; Stoick-Cooper et al., 2007; Wu et al., 2013).

The miRDeep2 program (Friedländer et al., 2012) was used to align and quantify miRNA reads. Most of the miRNAs that we detected during OS regeneration have been described previously (Hendrix et al., 2010; Keshavan et al., 2010; Missal et al., 2005; Norden-Krichmar et al., 2007; Shi et al., 2009; Terai et al., 2012); however, miRDeep2 also predicted 52 previously undescribed miRNAs (probability  $95 \pm 3\%$ ; Table S7). The most highly expressed of these novel miRNAs, *l\_2011*, was found to have an identical seed sequence to *hsa-miR-4709-5p* and was detected at >50-fold greater number of reads than the second most highly expressed novel miRNA. Another novel miRNA, *l2\_9033*, was found to be strongly and significantly upregulated during regeneration. Overall, out of the 550 known miRNAs in miRBase

(Griffiths-Jones, 2004; Kozomara and Griffiths-Jones, 2014) plus the novel miRNAs predicted by miRDeep2, we detected 279 miRNAs in the miRNA library reads at a threshold of  $\geq 1$  counts per million (CPM) in three or more samples. Comparisons were made between miRNA transcripts in the newly amputated siphon (D0) and each of the days of regeneration (D1, D3 and D8). Of the 279 miRNAs expressed, 15 and 23 were found to be DE on at least one of the days of regeneration by EdgeR and DESeq2, respectively. Of the DE miRNAs identified by EdgeR, 14 were also identified by DESeq2 (Table 1 and Table S3). In contrast to the mRNAs, there were approximately twice as many miRNAs significantly downregulated versus upregulated, suggesting an active role for miRNAs in adult OS homeostasis. The total number of DE transcripts for each day of regeneration is shown in Table 1.

Several DE miRNAs were also selected for validation based on their large estimated fold-change, significance of relative change, or previous reports indicating roles for these miRNAs in morphogenetic and regenerative processes (Fig. 2B). In regenerating OSs *miR-9* is highly upregulated at all stages of regeneration analyzed, having no RNAseq reads and being nearly undetectable by qRT-PCR at D0. Additionally, the bicistronic *miR-1/133* (Kusakabe et al., 2013), which has been implicated in muscle development and regeneration (Li et al., 2013; Mitchelson and Qin, 2015; Yin et al., 2008), was also upregulated during OS regeneration. In summary, the relative expression changes estimated by RNAseq for 9/15 mRNA transcripts (60%) were validated using qRT-PCR in at least one stage during regeneration. Likewise, we were able to validate that the levels of 10/17 miRNAs (58.8%) were significantly changed during at least one stage.

### Functional comparison between three stages of regeneration

In addition to identifying DE transcripts following amputation, enrichment for functional categories of genes was performed using classifications curated by the Gene Ontology (GO) Consortium (Ashburner et al., 2000) and the Kyoto Encyclopedia of Genes and Genomes (KEGG) Pathway Database (Kanehisa and Goto, 2000) (Table S8). Enrichment of functional categories based on the mean expression value (RPKM) of genes within each category in NR OS is shown in Fig. S2. Enrichment of functional categories based on the mean significance ( $-\log_2$  FDR) of genes within each category was performed by comparing the three days of regeneration (D1, D3 and D8) with either D0 (Fig. 3) or NR OSs (Fig. S3). The complete list of z-scores for all categories relative to either reference stage is listed in Table S9.

Several GO Biological Process (BP) categories showed a pattern of enrichment across all stages, including ‘negative regulation of peptidase activity’, ‘xenobiotic metabolic processes’, ‘protein folding’, ‘cellular calcium ion homeostasis’ and ‘multicellular organismal development’ (Fig. 3A). Similarly enriched GO Molecular Function (MF) categories included ‘peptidase inhibitor’, ‘heme binding’, ‘unfolded protein binding’ and ‘growth factor activity’ (Fig. 3B). For the most part, categories modified across the 8 days of regeneration studied are consistent with a pattern of activated cellular growth and metabolism.

Other categories were enriched during specific stages of regeneration. As expected, categories enriched early in regeneration (D1 and D3) included those related to wound healing, stress response, activation of morphogenetic processes and signaling. For example, the KEGG pathway ‘AGE-RAGE signaling in diabetic complications’ (which includes upregulated immune/stress-response genes like *JAK1*, *STAT5A* and *Jun*) was



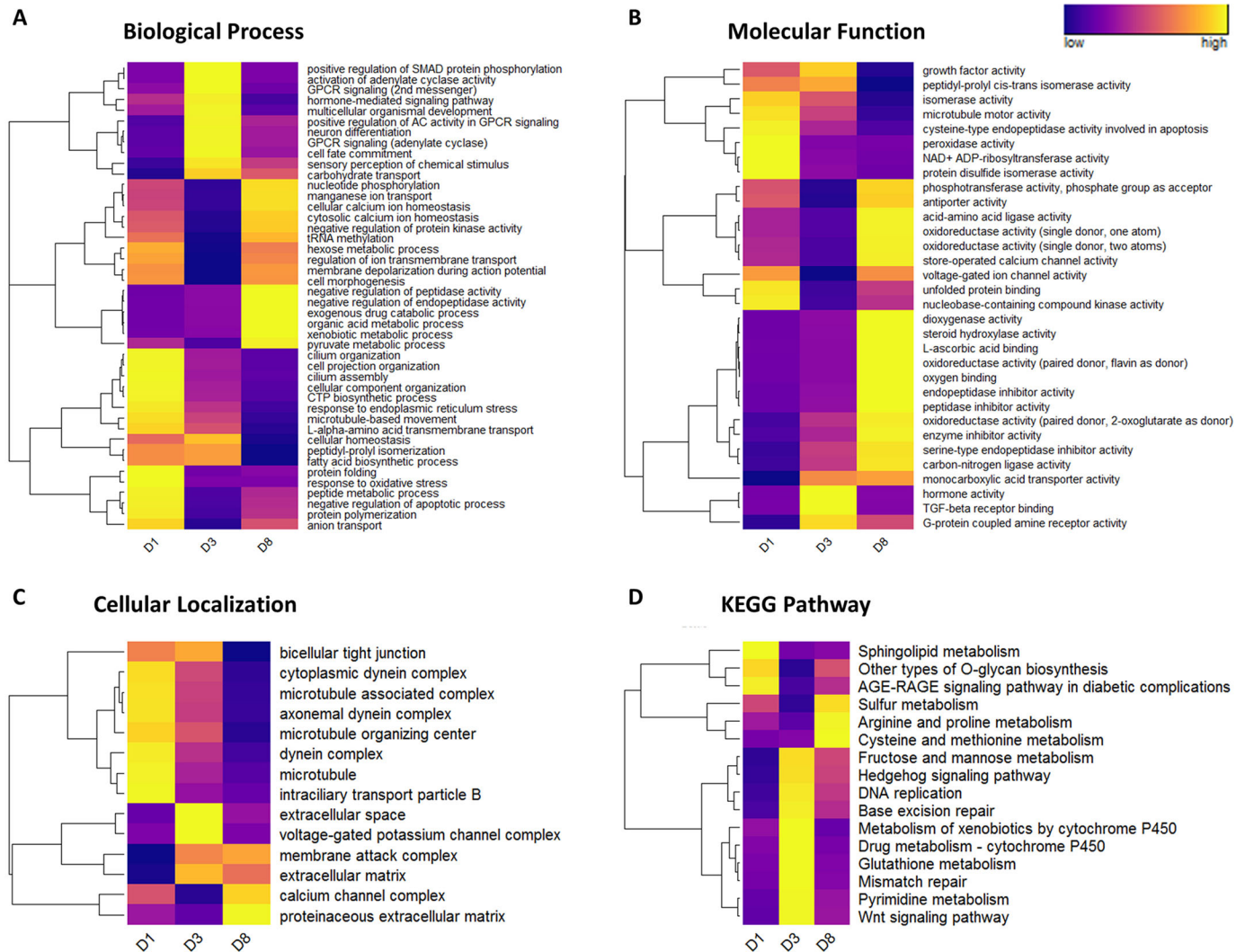


**Fig. 3. Standardized z-scores of enriched ( $z \geq 1.96$ ) functional categories.** z-scores, plotted as heatmaps, were calculated relative to D0 then standardized across post-amputation stages D1, D3 or D8. Dendrograms to the left of each heatmap indicate the results of hierarchical clustering of the indicated GO categories (A–C) or KEGG pathways (D).

enriched only at D1 (Fig. 3D). GO categories enriched exclusively at D1 include ‘response to endoplasmic reticulum stress’, ‘cilium organization’, ‘protein polymerization’, ‘steroid biosynthetic processes’ and ‘cysteine type endopeptidase activity involved in apoptosis’. Other categories enriched at both D1 and D3 include ‘microtubule-based movement and motor activity’, ‘hormone-mediated signaling’, ‘fatty acid biosynthesis’, ‘cellular homeostasis’ and ‘bicellular tight junction’.

Likewise, a number of categories with the potential to directly regulate morphogenetic processes during regeneration were enriched exclusively at D3. KEGG pathways enriched at this stage included ‘glutathione metabolism’, ‘DNA replication’ and ‘Wnt signaling’ (Fig. 3D). Corresponding GO categories enriched at this stage included ‘steroid hormone-mediated signaling’, ‘steroid hormone receptor activity’, ‘G-protein-coupled receptor activity’, ‘metalloendopeptidase activity’ and ‘voltage-gated potassium channel complex’.

Finally, categories enriched in later stages are expected to be involved in a return to homeostasis of the regenerating tissue, but could also represent downstream effects of changes observed at earlier stages and thus might not be exclusively enriched at late stage

expression. Categories enriched only at D8 appeared to be less associated with signaling pathways but instead more related to tissue growth, such as ‘glucose import’, ‘negative regulation of protein kinase activity’ and ‘amino acid transmembrane transporter activity’.

### Requirement of TGF $\beta$ signaling during early stages of regeneration

The increased expression of TGF $\beta$  activators observed post-amputation suggests a role for this signaling pathway in OS regeneration (Fig. 2). This was further supported by enrichment of functional categories related to TGF $\beta$  signaling at 3 days post-amputation (D) (Fig. 3A,B). It has been previously reported that TGF $\beta$  signaling is required for multiple events during regeneration of axolotl limbs, *Xenopus* tadpole tails and *Eublepharis* tails (Gilbert et al., 2013; Ho and Whitman, 2008; Lévesque et al., 2007). To investigate whether TGF $\beta$  is also required during OS regeneration, we treated amputated *C. robusta* juveniles with 10  $\mu$ M SB431542, a potent and specific inhibitor of activin receptor-like kinase receptors that mediate TGF $\beta$  signal transduction (Mita and Fujiwara, 2007).

Soaking *C. robusta* in SB431542 for 4 days following amputation completely blocked regeneration (Fig. 4). Whereas 100% of control-treated animals regenerated OPOs by 8 D, none of the SB431542-treated animals showed any visible signs of regeneration (Table 2). To further refine the temporal requirement for TGF $\beta$  signaling, we treated separate cohorts of animals with SB431542 over 24 h periods for each of the 4 days following amputation (Fig. 4A). Surprisingly, only the cohort treated over the first 24 h following amputation failed to regenerate completely, whereas the other three cohorts showed partial OPO regeneration (Table 2). The temporal requirement was further studied using three cohorts of animals treated with SB431542 for 48 h periods starting either (1) immediately after amputation, (2) 24 h after amputation or (3) 48 h after amputation (Fig. 4A). These 48 h treatments completely blocked regeneration in all cases (Fig. 4B), indicating that TGF $\beta$  signaling is required on at least two separate occasions during OS regeneration (once during a short window in the first 24 h, then again during a second >24 h window that includes 3 D).

### A network of miRNA target interactions

Here we report a non-biased correlation-based network to infer a comprehensive set of miRNA-target interactions over the course of 8 days of OS regeneration. Several transcriptome-wide miRNA profiling studies have been performed during limb or appendage regeneration (Gearhart et al., 2015; Holman et al., 2012; Thatcher et al., 2008), although not in parallel with mRNA transcriptome analysis. miRNAs primarily exert their effects on gene products through degradation or translational repression of target RNAs (Carthew and Sontheimer, 2009). In the absence of proteomic data, our analysis is limited to those cases in which miRNA-mRNA interactions result in degradation of the target mRNA (Carthew and Sontheimer, 2009). Assuming that an miRNA does result in degradation of a target transcript, the strength of miRNA-mRNA interactions can be estimated by identifying miRNA-target pairs that display inverse (negative) correlations between different stages of a process.

A preliminary step in this analysis required prediction of complementary sequence pairing between the full set of miRNAs (including novel miRNAs identified in this study) and the 3'-UTRs of potential target transcripts. We accomplished this using TargetScanS (Agarwal et al., 2015; Lewis et al., 2005), which was first employed to detect conserved binding sites between *C. robusta* and *C. savignyi*, before identifying additional non-conserved sites in non-orthologous genes. Our complete set of target predictions for *C. robusta* (conserved and non-conserved) contained ~521,000 pairwise interactions and is available for download (<https://labs.mcdm.ucsb.edu/smith/william>). Notably, within the conserved set of predictions between *C. robusta* and *C. savignyi* we identified the same 824 targets for *miR-124* as reported by another study (Chen et al., 2011), which identified miRNA seed pairing as a strong predictor of target downregulation in *Ciona*. Thus, we expect a large proportion of the predictions to be relevant *in vivo*. Further support for the relevance of these predictions was found by identifying a large proportion of the predicted miRNA-target pairs that are conserved with other species and have been validated experimentally (either by expression profiling, reporter assay or western blot) by comparing with information listed in miRTarBase (Chou et al., 2016) (data not shown).

The average log<sub>2</sub> fold-change estimated by DESeq2 and EdgeR at all stages (D0 versus D1, D3 or D8) was used to calculate Pearson correlation coefficients ( $\rho$ ) for all predicted miRNA-target pairs. Subsequent analysis was limited to miRNAs with observed changes  $\geq |1 \log_2\text{-fold}|$  at any stage and  $\rho \leq -0.9$  with their predicted targets. The resulting directed network contained 2033 nodes (129 miRNA, 1904 mRNA) and 2854 edges, with an average of 2.808 neighbors per node (Table S10). Evolution of biological networks is assumed to have proceeded by preferential attachment of new nodes to an existing core network, resulting in a 'scale-free' topology that can be modeled using a power law function (Albert, 2005; Barabási and Oltvai, 2004; Wolf et al., 2002). The in-degree distribution of edges/nodes was fitted to a power law curve with the equation  $y=2919.4x^{-3.362}$  ( $\rho=0.983$ ,  $R^2=0.917$ ), suggesting the

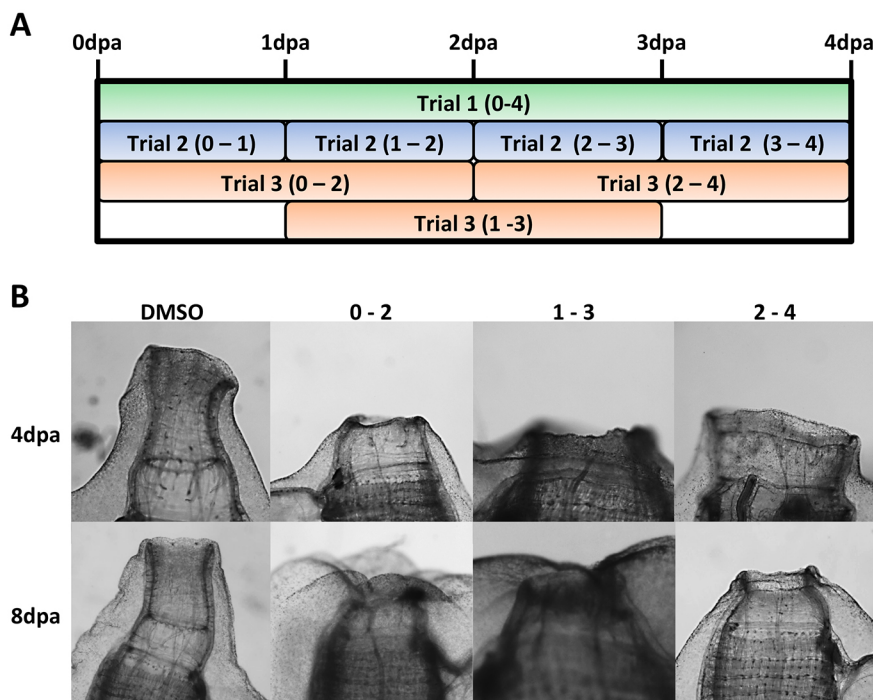


**Fig. 4. SB431542 treatment of *C. robusta* juveniles.** (A) Approximately 1-month-old animals were treated with 10  $\mu$ M SB431542 for the durations indicated. (B) Images of representative animals from the 48 h treatment cohorts (orange in A). DMSO, vehicle control. See also Table 2.

**Table 2. Number of animals with regenerated OPOs after SB431542 treatment**

| Cohort | Duration | 4 D   | 8 D   |
|--------|----------|-------|-------|
| DMSO   | 4 days   | 56/67 | 61/67 |
| 0-4    | 4 days   | 0/28  | 0/20  |
| 0-1    | 24 h     | 0/11  | 0/11  |
| 1-2    | 24 h     | 2/13  | 8/13  |
| 2-3    | 24 h     | 0/11  | 3/11  |
| 3-4    | 24 h     | 4/9   | 5/9   |
| 0-2    | 48 h     | 0/27  | 0/20  |
| 1-3    | 48 h     | 0/28  | 0/20  |
| 2-4    | 48 h     | 0/28  | 0/20  |

Cohort names correspond to conditions illustrated in Fig. 4A.

topology of our predicted network resembles that of a true biological network. Plotting these interactions shows a dense cluster of downregulated miRNAs associated with a dense cluster of upregulated mRNAs, joined by a few sparse connections (Fig. 5).

To assign putative functions to miRNAs within the correlation network, we implemented a clustering algorithm on all the nodes and then examined whether the list of targets in each cluster were enriched for particular GO categories and KEGG pathways. Non-overlapping clusters of miRNAs and targets were identified by analyzing the correlation network using the LinkLand algorithm (Kovács et al., 2010) provided by the ModuLand plug-in (Szalay-Bekő et al., 2012) for Cytoscape (Smoot et al., 2011). Briefly, each node is assigned a set of influence scores that relate it to all other nodes in the network based on their relative position and connections. Next, clusters are determined by identifying local maxima (which indicate the centers) and local minima (which define the boundaries) of influence scores throughout the network.

The miRNAs and targets assigned to each cluster are listed in Table S11. All of the targets within each resulting cluster were grouped and then the significance of overlap between each cluster and GO/KEGG functional categories was assessed using a hypergeometric test for enrichment (Table S12). Interpretations summarizing the significantly enriched functional categories are shown alongside their respective color-coded miRNA-target clusters in Fig. 5.

**DISCUSSION**  
**Molecular signatures indicate conserved features of regeneration**

Appendage regeneration is thought to occur in three morphologically distinct stages; wound healing, transition and redevelopment (Knapp et al., 2013). The wound healing stage is primarily defined by a localized immune response, closure of the epithelium and initiation of blastema formation (Murawala et al., 2012). We observed several transcriptional changes indicating conserved features of wound healing during OS regeneration. GO categories supporting this hypothesis that are enriched at D1 include ‘response to ER stress’, ‘response to oxidative stress’, ‘protein folding’, ‘unfolded protein binding’, ‘cysteine-type endopeptidase activity involved in apoptosis’ and the KEGG pathway ‘AGE-RAGE signaling pathway in diabetic complications’ (Fig. 3).

Following healing, a transition occurs in which the existing appendage begins to redevelop the lost tissue. During this transition phase, positional identity is regained and signaling to activate progenitor cells that are required to initiate growth occurs. Insulin growth factor (IGF) signaling was first implicated in limb regeneration in newts over three decades ago (Vethamany-Globus, 1987; Vethamany-Globus et al., 1984). More recently, it was

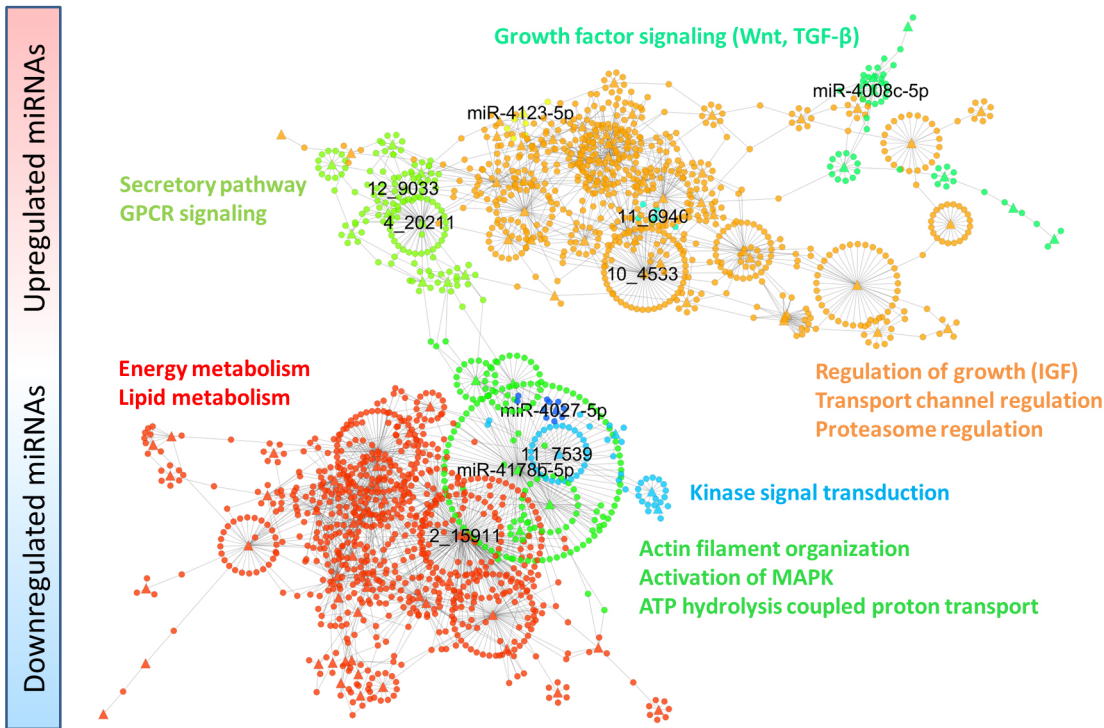


**Fig. 5. miRNA-mRNA correlation network.** miRNAs and mRNAs are represented by triangles and circles, respectively. Transcripts are joined by a line when both  $\rho \leq -0.9$  and a binding interaction was predicted by TargetScanS. ModuLand clusters are shown in different colors and the miRNA ID that defines each cluster is indicated (black text). Summary interpretations of enriched GO categories and KEGG pathways in each cluster are indicated in matching colors adjacent to the respective cluster. The full set of correlations, assignment of nodes to clusters and functional enrichments for clusters are listed in Table S12.



discovered that IGF secreted from wounded zebrafish epithelia stimulates underlying mesenchymal blastema cells to proliferate (Chablais and Jazwinska, 2010). Further, it has been hypothesized that a Warburg effect (Vander Heiden et al., 2009) can be promoted in regenerating vertebrate tissues to favor structural biosynthesis over generation of ATP (Love et al., 2014b). We observed high levels of *IGF* and *IGF binding protein (IGFbp)* transcript levels throughout regeneration (Fig. 2). IGF binding proteins have been reported to act as carriers for IGF to promote increased persistence of IGF in circulation (Hwa et al., 1999). Further investigation into the role of IGF signaling during OS regeneration could help determine whether the effects of this signaling pathway on cell proliferation and energy metabolism in different models of vertebrate regeneration are likely to be derived from a common evolutionary origin.

The transverse vessels of the branchial sac in *C. robusta* are thought to contain progenitor cells required for OS regeneration that are activated to proliferate and migrate into the OS after amputation (Jeffery, 2015b). Although the extent to which these branchial sac stem cells contribute to various tissues has not yet been investigated, it is suggested that they have the potential to differentiate into multiple lineages due to high expression of pluripotent cell marker genes such as *Piwi* and *Alkaline phosphatase* (Juliano et al., 2011, 2014; O'Connor et al., 2008; Štefková et al., 2015). *Piwi*-positive stem cells in colonial tunicates are essential for whole-body regeneration (Brown et al., 2009) and also originate from a vascular niche (Rinkevich et al., 2010). Cells of the branchial sac divide following amputation (Jeffery, 2015b); however, EdU and phospho-histone H2 labeling of regenerating OSs showed no detectable increase in the number of dividing cells per unit area until ~4 D (Auger et al., 2010). We observed transcriptional changes supporting the proposed timing of proliferation, such as the enrichment at D3 of the KEGG pathways 'DNA replication' and 'Wnt signaling' along with the GO categories 'TGFβ receptor binding', 'cell fate commitment' and 'growth factor activity' (Fig. 3).

Our identification of the requirement for TGFβ signaling at 3 D, as indicated by the lack of subsequent tissue regrowth and OPO differentiation following SB431542 treatment, as opposed to any potential disruption of patterning or the null hypothesis of no effect, further supports the hypothesis that a progenitor population is receiving inductive signals, putatively TGFβ itself, at this stage in order to stimulate proliferation and regeneration of lost tissue. Further studies comparing localization of TGFβ pathway members and effects on proliferation after SB431542 treatment during OS regeneration could identify the mechanism by which this pathway regulates regenerative regrowth and differentiation.

Once progenitor cells have been specified and positional identity within the regenerating tissue is established, the latter stages of regeneration are thought to proceed in a similar manner to how the original appendage/tissues were formed during development. This process involves extensive remodeling of the extracellular matrix (ECM) to regulate cellular responses such as apoptosis, proliferation, migration and differentiation (Calve et al., 2010; Lu et al., 2011). ECM remodeling is regulated via activation of specific enzymes such as Serpins (Simone et al., 2014) and TIMPs (Arpino et al., 2015), which inhibit peptidases that degrade structural ECM proteins. We observed strong enrichment of the GO categories 'peptidase inhibitor' and 'negative regulation of peptidase activity' at later stages of regeneration, particularly at D8 (Fig. 3). This supports the hypothesis that OS regeneration involves substantial ECM remodeling at early and mid stages, which is actively

attenuated by expression of peptidase inhibitors such as serpins and TIMPs at later stages.

A microarray-based study of gene expression during OS regeneration was recently published (Hamada et al., 2015). This study reported the 30 genes with the largest changes relative to NR OS at 3, 6 and 9 D. We compared the list of genes reported as DE at day 3 of regeneration with an analogous list derived in this study (Table S4). When converting from the gene identifiers used on the microarray, we were able to identify Ensembl gene models for 26 out of the 30 microarray probe sets listed. Of these Ensembl transcript models, 18/26 transcripts were expressed above the threshold of 5 RPKM in at least three or more samples, but only 6 of these 18 were identified as DE (FDR ≤ 0.05) by DESeq2, 5 of which were confirmed by EdgeR, notably including *Notch* and *EphA4*.

### Stage specificity of functional category overlap with miRNA-target clusters

We observed significant overlap between transcripts in certain functional categories and particular miRNA-target clusters. For example, categories related to 'immune response', 'stress responses' and 'apoptosis' were enriched at D1 relative to D0. These categories also significantly overlapped with miRNA-target clusters *miR-4178b-5p* and *4\_20211* (Table S12). Further, attenuation of apoptosis and induction of morphogenetic growth factor signaling are crucial for the transition from wound healing to the activation of redevelopment. Several miRNA clusters were found to target mRNAs annotated in functional categories related to Wnt, TGFβ and MAPK signaling, as well as regulation of apoptosis and regulation of cell cycle including *miR-4008c-5p*, *miR-4123-5p*, *miR-4178b-5p*, *2\_15911*, *4\_20211* and *11\_7539* (Table S12). Finally, during the redevelopment stage we observed strong enrichment of ECM peptidase inhibitors (Fig. 3), which significantly overlapped with the miRNA-target clusters *miR-4008c-5p*, *10\_4533* and *11\_6940*.

During all stages of regeneration we observed increased levels of *IGF* and *IGFbp* transcripts (Fig. 2A). The GO MF categories 'insulin receptor binding' and 'insulin-like growth factor binding' significantly overlapped with the miRNA-target cluster *10\_4533* (Table S12). Regulation of IGF-regulated processes by cluster *10\_4533* is further supported by significant overlap of its targets with the GO BP categories 'regulation of cell fate specification', 'regulation of cell growth' and 'regulation of mitotic cell cycle' (Table S12). This miRNA-target cluster might also be involved in regulating multiple unrelated processes at specific stages of regeneration. First, this cluster significantly overlaps with the categories 'unfolded protein binding' and 'regulation of apoptotic processes', which are enriched at the D1 stage (Fig. 3). Second, as mentioned previously, the miRNA-target cluster *10\_4533* significantly overlaps with the GO MF category 'endopeptidase inhibitor activity', which is highly enriched at D8 (Fig. 3).

We observed *miR-9*, an ancient and well-conserved miRNA essential for normal function of developing and differentiated neurons (Coolen et al., 2013), to be specifically upregulated during regeneration. This miRNA has previously been identified as expressed during the gastrula and larval stages of *C. robusta* (Hendrix et al., 2010). In other species *miR-9* has been shown to regulate differentiation via targeting of the Notch signaling pathway (Jing et al., 2011; Kuang et al., 2012). The proliferative state of neural progenitors is governed by oscillations in the protein level of Hes1; high levels of *miR-9* were shown to dampen oscillations of Hes1 leading to increased proliferation and differentiation (Bonev et al., 2012; Tan et al., 2012). Interestingly, we did not identify

binding sites for *miR-9* in any members of the Notch pathway or predicted downstream targets of *Hes1* (data not shown). However, our 17 predicted targets for *miR-9* do suggest a possible role in regulating differentiation and the proliferative state of neural progenitors through regulation of the cytoskeleton and cell cycle (Galderisi et al., 2003; McBeath et al., 2004). Functional categories significantly overlapping with *miR-9* network cluster targets that are associated with cell cycle regulation are ‘cell division’, ‘DNA replication initiation and DNA replication’, which contain the *miR-9* targets *Nek7-like*, *SFII-like* and *Myb-binding 1A*. Categories significantly overlapping with *miR-9* network clusters associated with cytoskeletal regulation are ‘intermediate filament’, ‘cytoskeleton organization’, ‘microtubule-based movement’, ‘microtubule motor activity’, ‘kinesin complex’ and ‘microtubule binding’, which include the *miR-9* targets *villin-1*, *Kinesin*, *sideroflexin-1-like*, *LIMK1-like*, *myosin X* and *LMNTD1*.

### Significance and limitations of the predicted miRNA-mRNA network

miRNA regulation is important in several well-studied examples of regeneration (Sen and Ghatak, 2015). miRNAs can either lead to direct degradation or translational repression of their target transcripts (Carthew and Sontheimer, 2009). One obvious caveat of miRNA and mRNA transcriptional profiling is that translational repression cannot be detected. If a given miRNA is predicted to target a given transcript based on seed pairing and the expression levels of these two transcripts are inversely correlated, we infer the predicted interaction is specific and results in target degradation. Predicted target pairs that do not show an inverse correlation could still result in translational repression; however, the relevance and extent of this type of interaction was not considered in this study.

For 8 of the 22 clusters detected by ModuLand (Fig. 5 and Table S11), the most central nodes identified as representing each cluster were novel miRNAs identified in this study. This underscores the complementary nature of co-expression and differential expression analyses. Co-expression analysis was able to identify individual miRNA(s) with small relative fold changes as important during regeneration by virtue of the position of that miRNA within a correlation network. On the other hand, differential expression analysis did not identify many novel miRNAs to be important during regeneration but was able to identify miRNAs that had the largest fold changes at any stage.

### Conclusions

Concurrent expression profiling of mRNA and miRNA has proven to be a useful approach for characterizing transcriptome-wide changes in gene expression during OS regeneration. We successfully identified a variety of transcriptional changes supporting the hypothesis that several major features of vertebrate appendage regeneration are conserved in *C. robusta*. Examples include categories of genes related to wound healing, proliferation, differentiation and ECM remodeling that were enriched at specific stages of regeneration. Further, we present a high-confidence network of miRNAs and their predicted targets during OS regeneration. This enabled subsequent annotation of putative miRNA functions during regeneration by virtue of identifying discrete clusters of miRNAs and their associated targets within the network. Several clusters of miRNAs and their targets were found to significantly overlap with functional categories that were likely to be involved in specific stages of OS regeneration owing to the preferential enrichment of these functional categories at specific stages.

This work provides a systematic characterization of mRNA and miRNA expression during OS regeneration, a comprehensive set of predicted interactions between these two gene product types and predicts effects of those interactions on cellular processes during regeneration – all of which are necessary to facilitate future investigation into the genetic requirements of appendage regeneration in chordates.

## MATERIALS AND METHODS

### Animal husbandry and RNA extraction

*C. robusta* were collected at the Santa Barbara Yacht Harbor. Gametes from two adults were mixed and the resulting offspring were grown to ~6 months of age. Approximately 75 sibling animals ranging in size from 5–10 cm were selected for amputation and anesthetized in 0.04% MS222 for 30 min. Amputated siphon samples were immediately frozen in liquid nitrogen then transferred to 1 ml RNAlater-ICE (Life Technologies) and stored at –20°C for 1 week. Total RNA was extracted from a pool of five tissue samples for each replicate using the miRvana Total RNA Extraction Kit (Life Technologies). During timecourse experiments, batches of animals were housed in five-gallon (~19 liter) buckets of seawater, changed daily and maintained at 15°C with a 12/12 h artificial light/dark cycle.

### RNA sequencing and data preprocessing

Poly(A)<sup>+</sup> RNA was isolated from 5 µg total RNA using Dynabeads (Life Technologies). Small RNAs (~18–30 nucleotides), including miRNAs, were isolated from 1 µg total RNA by 1% Tris-borate-EDTA acrylamide gel electrophoresis. Sequencing libraries were prepared with the Total RNAseq Kit v2.0 (Life Technologies). Libraries were sequenced in multiplex using an Ion Proton sequencer (Life Technologies). Raw reads were trimmed of adapter sequences and preprocessed for base quality according to the default software specifications. Further quality control was performed using FastQC and SamTools (Li et al., 2009). The *C. intestinalis* (now called *robusta*) JGI genome version 2.0 and Ensembl transcript models (release 83) were used as references for alignment. mRNA libraries were first aligned to the *C. robusta* genome and set of Ensembl transcript models using TopHat (Trapnell et al., 2009) with strict parameters (‘end-to-end’ mode) to accommodate spliced reads, then the initially unaligned reads were processed using Bowtie (Langmead et al., 2009) with relaxed parameters (‘local’ mode) to increase the overall robustness of alignment to the highly polymorphic *C. robusta* genome. HTseq-count (Anders et al., 2015) was used to count reads for each mRNA transcript. miRNA precursor sequences were downloaded from miRBase (Kozomara and Griffiths-Jones, 2014) and used along with the *C. robusta* genome by miRDeep2 (Friedländer et al., 2012) to align and quantify the miRNA libraries. Counts of novel miRNAs were extracted from the miRDeep2 output using a custom Python script.

### Differential expression, co-expression and enrichment analyses

mRNA samples were initially normalized for sequencing depth and transcript length (RPKM), whereas miRNA samples were first normalized only by sequencing depth (CPM). To reduce the number of tests performed, low and non-expressed genes were removed using filters of RPKM ≥ 5 or CPM ≥ 1 in at least three individual samples for mRNA and miRNA libraries, respectively. Normalization of counts and likelihood ratio tests were performed with the EdgeR and DESeq2 packages in R to determine differential expression relative to D0. Pairwise correlations ( $\rho \leq -0.9$ ) were calculated using R from log<sub>2</sub> fold-change values for mRNA and miRNA data sets estimated by DESeq2. To determine GO categories and KEGG pathways that were enriched at each stage relative to a reference stage (NR or D0), the mean –log<sub>2</sub> transformed FDR-adjusted *P*-value of each gene determined by EdgeR and DESeq2 was used as input for a two-tailed z-test (Maciejewski, 2013; Perez-Llomas and Lopez-Bigas, 2011). z-tests were performed using a 10,000 replicate bootstrap and FDR multiple testing adjustment using Gtools 2.2.3 (Perez-Llomas and Lopez-Bigas, 2011). Significance of overlap between miRNA targets and functional categories was performed using hypergeometric tests in R, with the resulting *P*-values corrected for multiple testing (FDR). For



overlap tests, lists or categories with fewer than five transcripts were removed to reduce false positives.

### qRT-PCR validation of relative expression

Custom TaqMan assays manufactured by Thermo Fisher were used for quantifying relative amounts of miRNA expression. SYBR Green detection was used for quantifying relative amounts of mRNA expression. All experiments were performed using a QuantStudio 1200K-Flex platform and analyzed using ExpressionSuite software (Applied Biosciences). mRNA expression levels were normalized to the geometric mean of *GAPDH* and *RNA polymerase 2*. Global normalization was used for miRNA expression levels because a sufficiently stable endogenous reference gene could not be identified despite testing several of the least variable genes from the deep-sequencing data. Primer sequences for mRNA detection were designed using BatchPrimer3 (You et al., 2008) and are listed in Table S5 along with Ensembl transcript identifiers and all gene names used in this study. The sequences of the miRNA detection probes are proprietary (Applied Biosystems) and not available to the researchers. One-way ANOVA was used to determine transcripts that were significantly DE during at least one stage of regeneration, as assessed by qRT-PCR (Table S6).

### miRNA target prediction

3'-UTR sequences and a paired list of orthologous genes for *C. robusta* and *C. savignyi* were downloaded from Ensemble Biomart; orthologous 3'-UTR sequences were then grouped according to the pairs of orthologous transcript IDs. Each resulting group of orthologous 3'-UTRs was aligned using Clustal Omega (Sievers et al., 2011) and then the resulting alignments were concatenated into a single file that included the remaining *C. robusta* 3'-UTRs that did not have orthologs in *C. savignyi*. The multiple alignment results were used with mature miRNA sequences downloaded from miRBase directly by TargetScanS (Lewis et al., 2005) to identify conserved seed regions for all *C. robusta* miRNAs (known and predicted in this study).

### Acknowledgements

We thank Dr Matthew Kourakis and Dr Erin Newman-Smith for helpful criticisms of this manuscript, and Dr Otto Guedelhofer and Dr Sarah Abdul Wajid for insight and feedback while designing experiments.

### Competing interests

The authors declare no competing or financial interests.

### Author contributions

Conceptualization: E.J.S., W.C.S., K.S.K.; Methodology: E.J.S., E.G., H.Z., W.C.S., K.S.K.; Software: E.J.S., H.Z.; Validation: E.J.S., E.G.; Investigation: E.J.S., E.G.; Formal analysis and investigation: E.J.S.; Writing - original draft preparation: E.J.S., W.C.S.; Writing - review and editing: E.J.S., W.C.S., K.S.K.; Funding acquisition: W.C.S.; Resources: W.C.S., K.S.K.; Supervision: W.C.S., K.S.K.

### Funding

This work was supported by the National Institutes of Health [HD038701 to W.C.S.]. Deposited in PMC for release after 12 months.

### Data availability

Raw and processed data (transcript counts) are available from the NCBI Gene Expression Omnibus repository under accession number GSE84837 (<http://www.ncbi.nlm.nih.gov/geo/query/acc.cgi?token=kwvtoqcutdwfz&acc=GSE84837>).

### Supplementary information

Supplementary information available online at <http://dev.biologists.org/lookup/doi/10.1242/dev.144097.supplemental>

### References

Agarwal, V., Bell, G. W., Nam, J.-W. and Bartel, D. P. (2015). Predicting effective microRNA target sites in mammalian mRNAs. *Elife* **4**, e05005.  
 Albert, R. (2005). Scale-free networks in cell biology. *J. Cell Sci.* **118**, 4947-4957.  
 Anders, S., Pyl, P. T. and Huber, W. (2015). HTSeq—a Python framework to work with high-throughput sequencing data. *Bioinformatics* **31**, 166-169.  
 Arpino, V., Brock, M. and Gill, S. E. (2015). The role of TIMPs in regulation of extracellular matrix proteolysis. *Matrix Biol.* **44-46**, 247-254.

Ashburner, M., Ball, C. A., Blake, J. A., Botstein, D., Butler, H., Cherry, J. M., Davis, A. P., Dolinski, K., Dwight, S. S., Eppig, J. T. et al. (2000). Gene ontology: tool for the unification of biology. *Nat. Genet.* **25**, 25-29.  
 Auger, H., Sasakura, Y., Joly, J.-S. and Jeffery, W. R. (2010). Regeneration of oral siphon pigment organs in the ascidian *Ciona intestinalis*. *Dev. Biol.* **339**, 374-389.  
 Barabási, A.-L. and Oltvai, Z. N. (2004). Network biology: understanding the cell's functional organization. *Nat. Rev. Genet.* **5**, 101-113.  
 Barker, N. (2014). Adult intestinal stem cells: critical drivers of epithelial homeostasis and regeneration. *Nat. Rev. Mol. Cell Biol.* **15**, 19-33.  
 Barker, N., Wetering, M. van de, and Clevers, H. (2008). The intestinal stem cell. *Genes Dev.* **22**, 1856-1864.  
 Bely, A. E. and Nyberg, K. G. (2010). Evolution of animal regeneration: re-emergence of a field. *Trends Ecol. Evol.* **25**, 161-170.  
 Bonev, B., Stanley, P. and Papalopulu, N. (2012). MicroRNA-9 modulates Hes1 ultradian oscillations by forming a double-negative feedback loop. *Cell Rep.* **2**, 10-18.  
 Brown, F. D., Keeling, E. L., Le, A. D. and Swalla, B. J. (2009). Whole body regeneration in a colonial ascidian, *Botrylloides violaceus*. *J. Exp. Zool. B Mol. Dev. Evol.* **312**, 885-900.  
 Brunetti, R., Gissi, C., Pennati, R., Caicci, F., Gasparini, F. and Manni, L. (2015). Morphological evidence that the molecularly determined *Ciona intestinalis* type A and type B are different species: *Ciona robusta* and *Ciona intestinalis*. *J. Zool. Syst. Evol. Res.* **53**, 186-193.  
 Busby, M. A., Stewart, C., Miller, C. A., Grzeda, K. R. and Marth, G. T. (2013). Scotty: a web tool for designing RNA-seq experiments to measure differential gene expression. *Bioinformatics* **29**, 656-657.  
 Calve, S., Odelberg, S. J. and Simon, H.-G. (2010). A transitional extracellular matrix instructs cell behavior during muscle regeneration. *Dev. Biol.* **344**, 259-271.  
 Campbell, L. J., Suárez-Castillo, E. C., Ortiz-Zuazaga, H., Knapp, D., Tanaka, E. M. and Crews, C. M. (2011). Gene expression profile of the regeneration epithelium during axolotl limb regeneration. *Dev. Dyn.* **240**, 1826-1840.  
 Carthew, R. W. and Sontheimer, E. J. (2009). Origins and mechanisms of miRNAs and siRNAs. *Cell* **136**, 642-655.  
 Chablais, F. and Jazwinska, A. (2010). IGF signaling between blastema and wound epidermis is required for fin regeneration. *Development* **137**, 871-879.  
 Chen, J. S., Pedro, M. S. and Zeller, R. W. (2011). miR-124 function during *Ciona intestinalis* neuronal development includes extensive interaction with the Notch signaling pathway. *Development* **138**, 4943-4953.  
 Chiba, S., Sasaki, A., Nakayama, A., Takamura, K. and Satoh, N. (2004). Development of *Ciona intestinalis* juveniles (through 2nd ascidian stage). *Zool. Sci.* **21**, 285-298.  
 Chou, C.-H., Chang, N.-W., Shrestha, S., Hsu, S.-D., Lin, Y.-L., Lee, W.-H., Yang, C.-D., Hong, H.-C., Wei, T.-Y., Tu, S.-T. et al. (2016). miRTarBase 2016: updates to the experimentally validated miRNA-target interactions database. *Nucleic Acids Res.* **44**, D239-D247.  
 Coolen, M., Katz, S. and Bally-Cuif, L. (2013). miR-9: a versatile regulator of neurogenesis. *Front. Cell. Neurosci.* **7**, 220.  
 Crow, K. D. and Wagner, G. P. (2006). What is the role of genome duplication in the evolution of complexity and diversity? *Mol. Biol. Evol.* **23**, 887-892.  
 Dehal, P. and Boore, J. L. (2005). Two rounds of whole genome duplication in the ancestral vertebrate. *PLoS Biol.* **3**, e314.  
 Dehal, P., Satou, Y., Campbell, R. K., Chapman, J., Degnan, B., Tomaso, A. D., Davidson, B., Gregorio, A. D., Gelpke, M., Goodstein, D. M. et al. (2002). The draft genome of *Ciona intestinalis*: insights into chordate and vertebrate origins. *Science* **298**, 2157-2167.  
 Delsuc, F., Brinkmann, H., Chourrout, D. and Philippe, H. (2006). Tunicates and not cephalochordates are the closest living relatives of vertebrates. *Nature* **439**, 965-968.  
 Endo, T., Bryant, S. V. and Gardiner, D. M. (2004). A stepwise model system for limb regeneration. *Dev. Biol.* **270**, 135-145.  
 Friedländer, M. R., Mackowiak, S. D., Li, N., Chen, W. and Rajewsky, N. (2012). miRDeep2 accurately identifies known and hundreds of novel microRNA genes in seven animal clades. *Nucleic Acids Res.* **40**, 37-52.  
 Galderisi, U., Jori, F. P. and Giordano, A. (2003). Cell cycle regulation and neural differentiation. *Oncogene* **22**, 5208-5219.  
 Gearhart, M. D., Erickson, J. R., Walsh, A. and Echeverri, K. (2015). Identification of conserved and novel microRNAs during tail regeneration in the mexican axolotl. *Int. J. Mol. Sci.* **16**, 22046-22061.  
 Gilbert, R. W. D., Vickaryous, M. K. and Vitoria-Petit, A. M. (2013). Characterization of TGF $\beta$  signaling during tail regeneration in the leopard gecko (*Eublepharis macularius*). *Dev. Dyn.* **242**, 886-896.  
 Godwin, J. W., Pinto, A. R. and Rosenthal, N. A. (2013). Macrophages are required for adult salamander limb regeneration. *Proc. Natl. Acad. Sci. USA* **110**, 9415-9420.  
 Griffiths-Jones, S. (2004). The microRNA registry. *Nucleic Acids Res.* **32**, D109-D111.  
 Hamada, M., Goricki, S., Byerly, M. S., Satoh, N. and Jeffery, W. R. (2015). Evolution of the chordate regeneration blastema: Differential gene expression and conserved role of notch signaling during siphon regeneration in the ascidian *Ciona*. *Dev. Biol.* **405**, 304-315.

- Harty, M., Neff, A. W., King, M. W. and Mescher, A. L. (2003). Regeneration or scarring: an immunologic perspective. *Dev. Dyn.* **226**, 268-279.
- Hendrix, D., Levine, M. and Shi, W. (2010). miRTRAP, a computational method for the systematic identification of miRNAs from high throughput sequencing data. *Genome Biol.* **11**, R39.
- Ho, D. M. and Whitman, M. (2008). TGF-beta signaling is required for multiple processes during *Xenopus* tail regeneration. *Dev. Biol.* **315**, 203-216.
- Holman, E. C., Campbell, L. J., Hines, J. and Crews, C. M. (2012). Microarray analysis of microRNA expression during axolotl limb regeneration. *PLoS ONE* **7**, e41804.
- Hutchins, E. D., Eckalbar, W. L., Wolter, J. M., Mangone, M. and Kusumi, K. (2016). Differential expression of conserved and novel microRNAs during tail regeneration in the lizard *Anolis carolinensis*. *BMC Genomics* **17**, 339.
- Hwa, V., Oh, Y. and Rosenfeld, R. G. (1999). The insulin-like growth factor-binding protein (IGFBP) superfamily. *Endocr. Rev.* **20**, 761-787.
- Jeffery, W. R. (2015a). Closing the wounds: one hundred and twenty five years of regenerative biology in the ascidian *Ciona intestinalis*. *Genesis* **53**, 48-65.
- Jeffery, W. R. (2015b). Distal regeneration involves the age dependent activity of branchial sac stem cells in the ascidian *Ciona intestinalis*. *Regeneration* **2**, 1-18.
- Jhamb, D., Rao, N., Milner, D. J., Song, F., Cameron, J. A., Stocum, D. L. and Palakal, M. J. (2011). Network based transcription factor analysis of regenerating axolotl limbs. *BMC Bioinformatics* **12**, 80.
- Jing, L., Jia, Y., Lu, J., Han, R., Li, J., Wang, S., Peng, T. and Jia, Y. (2011). MicroRNA-9 promotes differentiation of mouse bone mesenchymal stem cells into neurons by Notch signaling. *Neuroreport* **22**, 206-211.
- Juliano, C., Wang, J. and Lin, H. (2011). Uniting germline and stem cells: the function of Piwi proteins and the piRNA pathway in diverse organisms. *Annu. Rev. Genet.* **45**, 447-469.
- Juliano, C. E., Reich, A., Liu, N., Götzfried, J., Zhong, M., Uman, S., Reenan, R. A., Wessel, G. M., Steele, R. E. and Lin, H. (2014). PIWI proteins and PIWI-interacting RNAs function in Hydra somatic stem cells. *Proc. Natl. Acad. Sci. USA* **111**, 337-342.
- Kanehisa, M. and Goto, S. (2000). KEGG: kyoto encyclopedia of genes and genomes. *Nucleic Acids Res.* **28**, 27-30.
- Keshavan, R., Virata, M., Keshavan, A. and Zeller, R. W. (2010). Computational identification of *Ciona intestinalis* microRNAs. *Zool. Sci.* **27**, 162-170.
- King, R. S. and Newmark, P. A. (2012). The cell biology of regeneration. *J. Cell Biol.* **196**, 553-562.
- Knapp, D., Schulz, H., Rascon, C. A., Volkmer, M., Scholz, J., Nacu, E., Le, M., Novozhilov, S., Tazaki, A., Protze, S. et al. (2013). Comparative transcriptional profiling of the axolotl limb identifies a tripartite regeneration-specific gene program. *PLoS ONE* **8**, e61352.
- Kovács, I. A., Palotai, R., Szalay, M. S. and Csermely, P. (2010). Community landscapes: an integrative approach to determine overlapping network module hierarchy, identify key nodes and predict network dynamics. *PLoS ONE* **5**, e12528.
- Kozomara, A. and Griffiths-Jones, S. (2014). miRBase: annotating high confidence microRNAs using deep sequencing data. *Nucleic Acids Res.* **42**, D68-D73.
- Kuang, Y., Liu, Q., Shu, X., Zhang, C., Huang, N., Li, J., Jiang, M. and Li, H. (2012). Dicer1 and MiR-9 are required for proper Notch1 signaling and the Bergmann glial phenotype in the developing mouse cerebellum. *Glia* **60**, 1734-1746.
- Kürn, U., Rendulic, S., Tiozzo, S. and Lauzon, R. J. (2011). Asexual propagation and regeneration in colonial ascidians. *Biol. Bull.* **221**, 43-61.
- Kusakabe, R., Tani, S., Nishitsuji, K., Shindo, M., Okamura, K., Miyamoto, Y., Nakai, K., Suzuki, Y., Kusakabe, T. G. and Inoue, K. (2013). Characterization of the compact bicistronic microRNA precursor, miR-1/miR-133, expressed specifically in *Ciona* muscle tissues. *Gene Expr. Patterns* **13**, 43-50.
- Langmead, B., Trapnell, C., Pop, M. and Salzberg, S. L. (2009). Ultrafast and memory-efficient alignment of short DNA sequences to the human genome. *Genome Biol.* **10**, R25.
- Lévesque, M., Gatién, S., Finnson, K., Desmeules, S., Villiard, É., Pilote, M., Philip, A. and Roy, S. (2007). Transforming growth factor:  $\beta$  signaling is essential for limb regeneration in axolotls. *PLoS ONE* **2**, e1227.
- Lewis, B. P., Burge, C. B. and Bartel, D. P. (2005). Conserved seed pairing, often flanked by adenosines, indicates that thousands of human genes are microRNA targets. *Cell* **120**, 15-20.
- Li, H., Handsaker, B., Wysoker, A., Fennell, T., Ruan, J., Homer, N., Marth, G., Abecasis, G. and Durbin, R., 1000 Genome Project Data Processing Subgroup (2009). The sequence alignment/map format and SAMtools. *Bioinformatics* **25**, 2078-2079.
- Li, Q., Guo, J., Lin, X., Yang, X., Ma, Y., Fan, G.-C. and Chang, J. (2013). An intragenic SRF-dependent regulatory motif directs cardiac-specific microRNA-1-1/133a-2 expression. *PLoS ONE* **8**, e75470.
- Love, N. R., Chen, Y., Bonev, B., Gilchrist, M. J., Fairclough, L., Lea, R., Mohun, T. J., Paredes, R., Zeef, L. A. and Amaya, E. (2011). Genome-wide analysis of gene expression during *Xenopus tropicalis* tadpole tail regeneration. *BMC Dev. Biol.* **11**, 70.
- Love, M. I., Huber, W. and Anders, S. (2014a). Moderated estimation of fold change and dispersion for RNA-seq data with DESeq2. *Genome Biol.* **15**.
- Love, N. R., Ziegler, M., Chen, Y. and Amaya, E. (2014b). Carbohydrate metabolism during vertebrate appendage regeneration: what is its role? how is it regulated? *BioEssays* **36**, 27-33.
- Lu, P., Takai, K., Weaver, V. M., Werb, Z. (2011). Extracellular matrix degradation and remodeling in development and disease. *Cold Spring Harb. Perspect. Biol.* **3**, pii: a005058.
- Maciejewski, H. (2013). Gene set analysis methods: statistical models and methodological differences. *Brief. Bioinform.* **15**, 504-518.
- McBeath, R., Pirone, D. M., Nelson, C. M., Bhadriraju, K. and Chen, C. S. (2004). Cell shape, cytoskeletal tension, and RhoA regulate stem cell lineage commitment. *Dev. Cell* **6**, 483-495.
- Missal, K., Rose, D. and Stadler, P. F. (2005). Non-coding RNAs in *Ciona intestinalis*. *Bioinformatics* **21** Suppl. 2, ii77-ii78.
- Mitchelson, K. R. and Qin, W.-Y. (2015). Roles of the canonical myomiRs miR-1, -133 and -206 in cell development and disease. *World J. Biol. Chem.* **6**, 162-208.
- Monaghan, J. R., Epp, L. G., Putta, S., Page, R. B., Walker, J. A., Beachy, C. K., Zhu, W., Pao, G. M., Verma, I. M., Hunter, T. et al. (2009). Microarray and cDNA sequence analysis of transcription during nerve-dependent limb regeneration. *BMC Biol.* **7**, 1.
- Morgan, T. H. (1901). *Regeneration*. New York: Macmillan.
- Murawala, P., Tanaka, E. M. and Currie, J. D. (2012). Regeneration: the ultimate example of wound healing. *Semin. Cell Dev. Biol.* **23**, 954-962.
- Norden-Krichmar, T. M., Holtz, J., Pasquinelli, A. E. and Gaasterland, T. (2007). Computational prediction and experimental validation of *Ciona intestinalis* microRNA genes. *BMC Genomics* **8**, 445.
- O'Connor, M. D., Kardel, M. D., Iosifina, I., Youssef, D., Lu, M., Li, M. M., Vercauteren, S., Nagy, A. and Eaves, C. J. (2008). Alkaline phosphatase-positive colony formation is a sensitive, specific, and quantitative indicator of undifferentiated human embryonic stem cells. *Stem Cells* **26**, 1109-1116.
- Perez-Llamas, C. and Lopez-Bigas, N. (2011). Gitoools: analysis and visualisation of genomic data using interactive heat-maps. *PLoS ONE* **6**, e19541.
- Rao, N., Jhamb, D., Milner, D. J., Li, B., Song, F., Wang, M., Voss, S. R., Palakal, M., King, M. W., Saranjami, B. et al. (2009). Proteomic analysis of blastema formation in regenerating axolotl limbs. *BMC Biol.* **7**, 83.
- Reddien, P. W. and Sánchez Alvarado, A. (2004). Fundamentals of planarian regeneration. *Annu. Rev. Cell Dev. Biol.* **20**, 725-757.
- Rinkevich, B. and Rinkevich, Y. (2012). The "Stars and Stripes" metaphor for animal regeneration-elucidating two fundamental strategies along a continuum. *Cells* **2**, 1-18.
- Rinkevich, B., Shlemberg, Z. and Fishelson, L. (1995). Whole-body protochordate regeneration from totipotent blood cells. *Proc. Natl. Acad. Sci. USA* **92**, 7695-7699.
- Rinkevich, Y., Rosner, A., Rabinowitz, C., Lapidot, Z., Moiseeva, E. and Rinkevich, B. (2010). Piwi positive cells that line the vasculature epithelium, underlie whole body regeneration in a basal chordate. *Dev. Biol.* **345**, 94-104.
- Robinson, M. D., McCarthy, D. J. and Smyth, G. K. (2010). edgeR: a Bioconductor package for differential expression analysis of digital gene expression data. *Bioinformatics* **26**, 139-140.
- Robles, J. A., Qureshi, S. E., Stephen, S. J., Wilson, S. R., Burden, C. J. and Taylor, J. M. (2012). Efficient experimental design and analysis strategies for the detection of differential expression using RNA-sequencing. *BMC Genomics* **13**, 484.
- Satou, Y., Mineta, K., Ogasawara, M., Sasakura, Y., Shoguchi, E., Ueno, K., Yamada, L., Matsumoto, J., Wasserscheid, J., Dewar, K. et al. (2008). Improved genome assembly and evidence-based global gene model set for the chordate *Ciona intestinalis*: new insight into intron and operon populations. *Genome Biol.* **9**, R152.
- Schebesta, M., Lien, C.-L., Engel, F. B. and Keating, M. T. (2006). Transcriptional profiling of caudal fin regeneration in zebrafish. *ScientificWorldJournal* **6** Suppl. 1, 38-54.
- Seifert, A. W., Monaghan, J. R., Voss, S. R. and Maden, M. (2012). Skin regeneration in adult axolotls: a blueprint for scar-free healing in vertebrates. *PLoS ONE* **7**, e32875.
- Sen, C. K. and Ghatak, S. (2015). miRNA control of tissue repair and regeneration. *Am. J. Pathol.* **185**, 2629-2640.
- Shi, W., Hendrix, D., Levine, M. and Haley, B. (2009). A distinct class of small RNAs arises from pre-miRNA-proximal regions in a simple chordate. *Nat. Struct. Mol. Biol.* **16**, 183-189.
- Sievers, F., Wilm, A., Dineen, D., Gibson, T. J., Karplus, K., Li, W., Lopez, R., McWilliam, H., Remmert, M., Söding, J. et al. (2011). Fast, scalable generation of high-quality protein multiple sequence alignments using Clustal Omega. *Mol. Syst. Biol.* **7**, 539.
- Simone, T. M., Higgins, C. E., Czekay, R.-P., Law, B. K., Higgins, S. P., Archambeault, J., Kutz, S. M. and Higgins, P. J. (2014). SERPINE1: a molecular switch in the proliferation-migration dichotomy in wound-"activated" keratinocytes. *Adv. Wound Care* **3**, 281-290.

- Smoot, M. E., Ono, K., Ruscheinski, J., Wang, P.-L. and Ideker, T. (2011). Cytoscape 2.8: new features for data integration and network visualization. *Bioinformatics* **27**, 431-432.
- Štefková, K., Procházková, J. and Pacherník, J. (2015). Alkaline phosphatase in stem cells. *Stem Cells Int.* **2015**, e628368.
- Stewart, R., Rascón, C. A., Tian, S., Nie, J., Barry, C., Chu, L.-F., Ardalani, H., Wagner, R. J., Probasco, M. D., Bolin, J. M. et al. (2013). Comparative RNA-seq analysis in the unsequenced axolotl: the oncogene burst highlights early gene expression in the blastema. *PLoS Comput. Biol.* **9**, e1002936.
- Stoick-Cooper, C. L., Moon, R. T. and Weidinger, G. (2007). Advances in signaling in vertebrate regeneration as a prelude to regenerative medicine. *Genes Dev.* **21**, 1292-1315.
- Szalay-Bekő, M., Palotai, R., Szappanos, B., Kovács, I. A., Papp, B. and Csérmely, P. (2012). ModuLand plug-in for Cytoscape: determination of hierarchical layers of overlapping network modules and community centrality. *Bioinformatics* **28**, 2202-2204.
- Tan, S.-L., Ohtsuka, T., González, A. and Kageyama, R. (2012). MicroRNA9 regulates neural stem cell differentiation by controlling Hes1 expression dynamics in the developing brain. *Genes Cells* **17**, 952-961.
- Terai, G., Okida, H., Asai, K. and Mituyama, T. (2012). Prediction of conserved precursors of miRNAs and their mature forms by integrating position-specific structural features. *PLoS ONE* **7**, e44314.
- Thatcher, E. J., Paydar, I., Anderson, K. K. and Patton, J. G. (2008). Regulation of zebrafish fin regeneration by microRNAs. *Proc. Natl. Acad. Sci. USA* **105**, 18384-18389.
- Tiozzo, S. and Copley, R. R. (2015). Reconsidering regeneration in metazoans: an evo-devo approach. *Evol. Dev. Biol.* **3**, 67.
- Trapnell, C., Pachter, L. and Salzberg, S. L. (2009). TopHat: discovering splice junctions with RNA-seq. *Bioinformatics* **25**, 1105-1111.
- Vander Heiden, M. G., Cantley, L. C. and Thompson, C. B. (2009). Understanding the warburg effect: the metabolic requirements of cell proliferation. *Science* **324**, 1029-1033.
- Vethamany-Globus, S. (1987). Hormone action in newt limb regeneration: insulin and endorphins. *Biochem. Cell Biol.* **65**, 730-738.
- Vethamany-Globus, S., Globus, M., Darch, A., Milton, G. and Tomlinson, B. L. (1984). In vitro effects of insulin on macromolecular events in newt limb regeneration blastemata. *J. Exp. Zool.* **231**, 63-74.
- Voskoboynik, A., Simon-Blecher, N., Soen, Y., Rinkevich, B., Tomaso, A. W. D., Ishizuka, K. J. and Weissman, I. L. (2007). Striving for normality: whole body regeneration through a series of abnormal generations. *FASEB J.* **21**, 1335-1344.
- Wolf, Y. I., Kerev, G. and Koonin, E. V. (2002). Scale-free networks in biology: new insights into the fundamentals of evolution? *BioEssays* **24**, 105-109.
- Wu, C.-H., Tsai, M.-H., Ho, C.-C., Chen, C.-Y. and Lee, H.-S. (2013). De novo transcriptome sequencing of axolotl blastema for identification of differentially expressed genes during limb regeneration. *BMC Genomics* **14**, 434.
- Yin, V. P., Thomson, J. M., Thummel, R., Hyde, D. R., Hammond, S. M. and Poss, K. D. (2008). Fgf-dependent depletion of microRNA-133 promotes appendage regeneration in zebrafish. *Genes Dev.* **22**, 728-733.
- You, F. M., Huo, N., Gu, Y. Q., Luo, M.-C., Ma, Y., Hane, D., Lazo, G. R., Dvorak, J. and Anderson, O. D. (2008). BatchPrimer3: a high throughput web application for PCR and sequencing primer design. *BMC Bioinformatics* **9**, 253.



## Supporting Information for “A microRNA-mRNA Expression Network during Oral Siphon Regeneration in *Ciona*”

Elijah J. Spina, Elmer Guzman, Hongjun Zhou, Kenneth S. Kosik, and William C. Smith

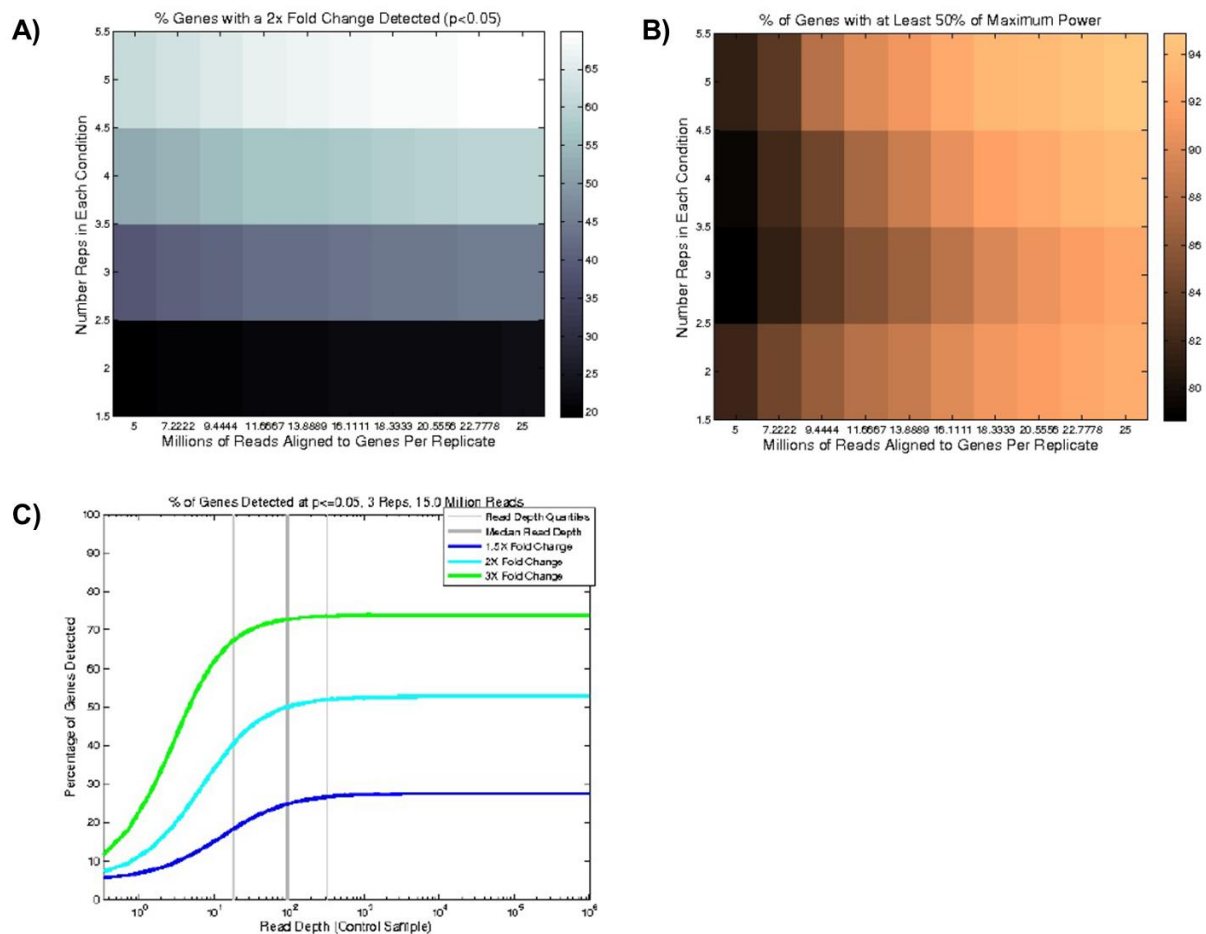


**Fig. S1. Pilot Study and Power Analysis of Non-Regenerating Oral Siphons.** (A) Power of different experimental designs. Power is measured by the percentage of transcripts having a true 2X fold change detected at  $p \leq 0.05$  using a t-test. (B) Measurement bias of different experimental designs. Maximum power is defined as the percentage of transcripts that could be detected if continuous sampling was performed. Then, measurement bias is defined as the percentage of transcripts sampled with at least 50% of the maximum power. (C) Expected true positive rates for our chosen experimental design. Curves indicate percent of differentially expressed transcripts expected to be detected at different levels of fold-change.

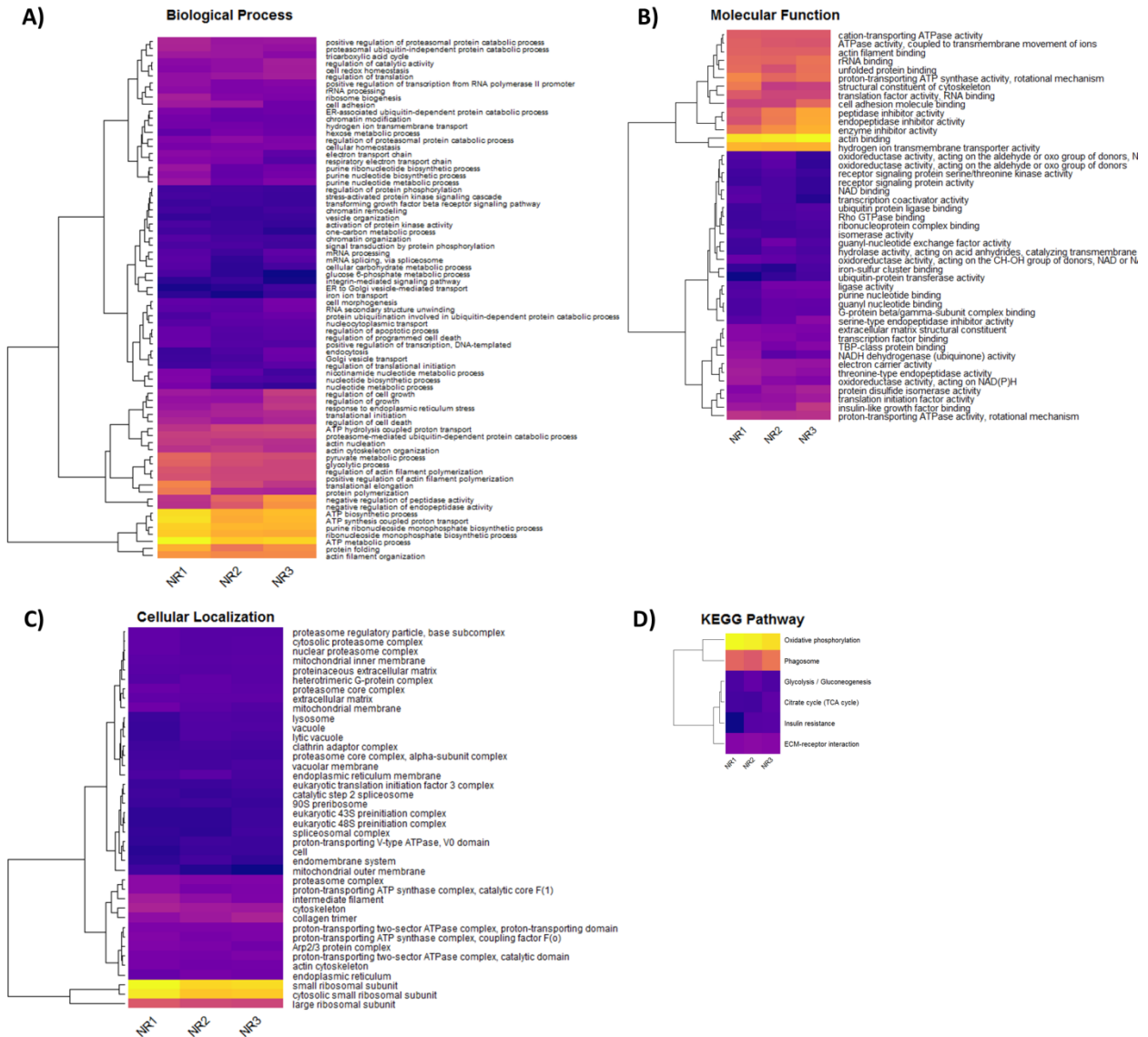


**Fig. S2. Z-scores of Enriched ( $Z \geq 1.96$ ) Functional Categories in Non-Regenerating Oral Siphons.** Z-scores plotted here as heatmaps were calculated using expression values normalized by transcript length and sequencing depth (RPKM). Dendrograms to the left of each heatmap indicate the results of hierarchical clustering the categories. Stages are listed below each column of the heatmaps while categories are listed to the right. (A) GO Biological Process. (B) GO Molecular Function. (C) GO Cellular Localization. (D) KEGG Pathways.

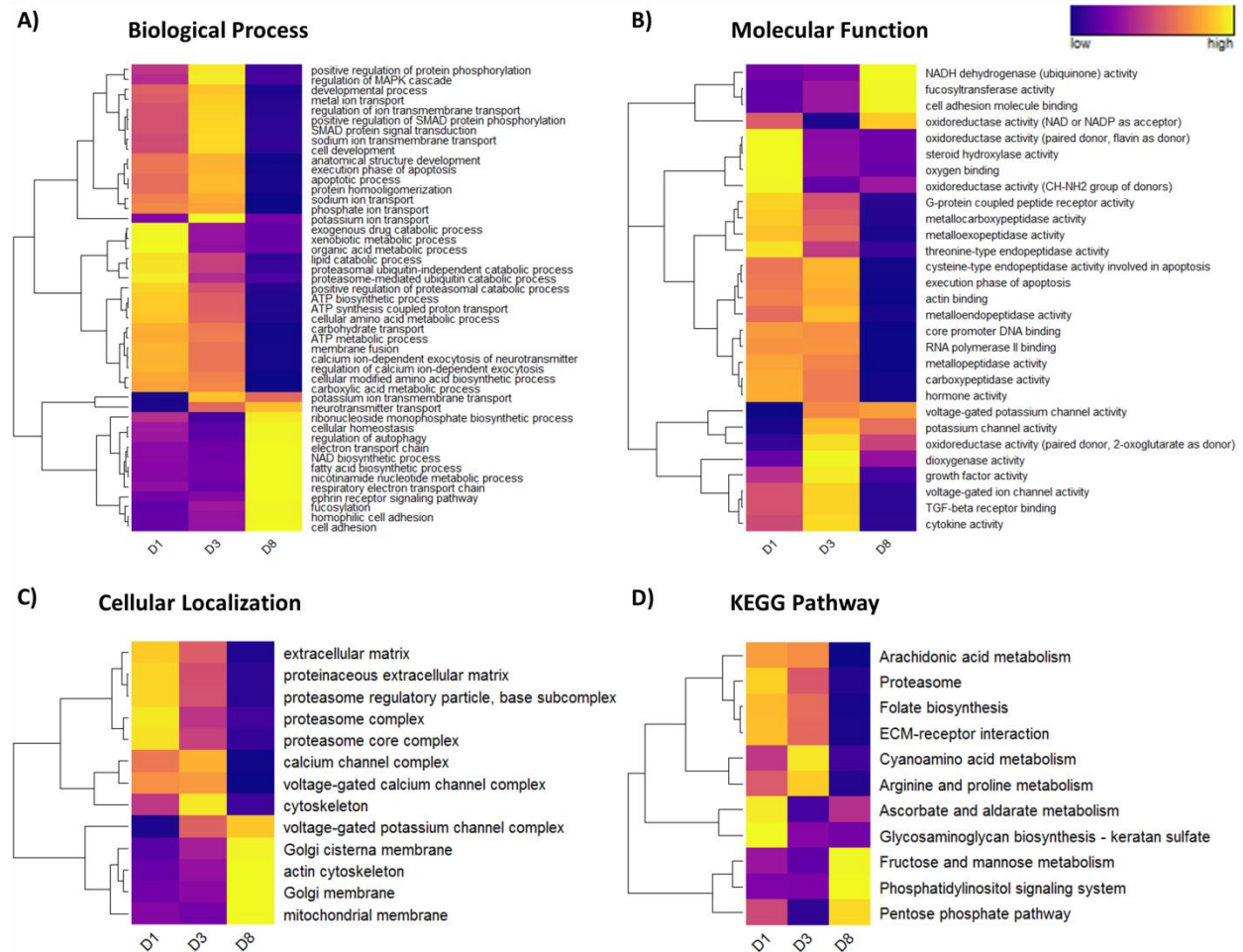


**Fig. S3. Z-scores of Enriched ( $Z \geq 1.96$ ) Functional Categories Relative to Non-Regenerating Oral Siphons.** Z-scores plotted here as heatmaps were calculated relative to non-regenerating (NR) oral siphon samples then standardized relative to the mean & standard deviation across stages. Dendrograms to the left of each heatmap indicate the results of hierarchical clustering the categories. Stages are listed below each column of the heatmaps while categories are listed to the right. (A) GO Biological Process. (B) GO Molecular Function. (C) GO Cellular Localization. (D) KEGG Pathways.



**Table S1. mRNA Alignment Statistics.** Alignment metrics are indicated in the first column. Each subsequent column represents one biological replicate sample. There are three replicates for each stage. Each sample is indicated by the stage symbol followed by a dash then the replicate number. Stage symbols are: NR = Non-regenerating, D0 = zero days post-amputation (dpa), D1 = one dpa, D3 = three dpa, D8 = eight dpa.

|                    | NR-1     | NR-2     | NR-3     | D0-1     | D0-2     | D0-3     | D1-1     | D1-2     | D1-3     | D3-1     | D3-2     | D3-3     | D8-1     | D8-2     | D8-3     |
|--------------------|----------|----------|----------|----------|----------|----------|----------|----------|----------|----------|----------|----------|----------|----------|----------|
| <b>Reads</b>       | 13036680 | 26048685 | 10107734 | 14707066 | 18649484 | 15964357 | 14334056 | 17302978 | 18405471 | 7081310  | 13860083 | 13753071 | 13303927 | 17968744 | 13076712 |
| <b>Non Primary</b> | 958540   | 1950057  | 737770   | 853845   | 729117   | 740310   | 855498   | 787854   | 1117746  | 121837   | 560209   | 676350   | 766385   | 681277   | 558519   |
| <b>Non-unique</b>  | 3956018  | 7294169  | 4316581  | 3973598  | 5973678  | 5559482  | 5680532  | 6179078  | 5482153  | 3500352  | 6855210  | 6101267  | 6578039  | 9854070  | 5993090  |
| <b>Unique</b>      | 8122122  | 16804459 | 5053383  | 9879623  | 11946689 | 9664565  | 7798026  | 10336046 | 11805572 | 3459121  | 6444664  | 6975454  | 5959503  | 7433397  | 6525103  |
| <b>Plus</b>        | 4067620  | 8854160  | 2612935  | 4791899  | 5787943  | 4577185  | 3938708  | 5160326  | 6006877  | 1759025  | 3286526  | 3306156  | 3001168  | 3726230  | 3182975  |
| <b>Minus</b>       | 4054502  | 7950299  | 2440448  | 5087724  | 6158746  | 5087380  | 3859318  | 5175720  | 5798695  | 1700096  | 3158138  | 3669298  | 2958335  | 3707167  | 3342128  |
| <b>Non-splice</b>  | 6257177  | 12295110 | 3922418  | 7151978  | 8014248  | 6969439  | 5557248  | 7172939  | 8415632  | 2563042  | 4458957  | 5079744  | 4288119  | 5168147  | 4787742  |
| <b>Splice</b>      | 1864945  | 4509349  | 1130965  | 2727645  | 3932441  | 2695126  | 2240778  | 3163107  | 3389940  | 896079   | 1985707  | 1895710  | 1671384  | 2265250  | 1737361  |
| <b>% Aligned</b>   | 0.926474 | 0.925138 | 0.927009 | 0.941943 | 0.960904 | 0.953627 | 0.940317 | 0.954467 | 0.939271 | 0.982795 | 0.959581 | 0.950822 | 0.942394 | 0.962085 | 0.957289 |
| <b>% Unique</b>    | 0.672465 | 0.69732  | 0.539317 | 0.713164 | 0.666654 | 0.634822 | 0.57855  | 0.625853 | 0.682888 | 0.497038 | 0.484566 | 0.533425 | 0.475333 | 0.429988 | 0.52125  |

**Table S2. Concurrence of Differentially Expressed mRNAs Between Two Programs relative to Day 0.** Results from EdgeR are shown after retaining only transcripts identified as differentially expressed by both EdgeR and DESeq2. Transcripts are indicated in the first column. Subsequent columns show the estimated log<sub>2</sub> fold-change (logFC) for each stage (D1 = one dpa, D3 = three dpa, D8 = eight dpa), the mean log<sub>2</sub> counts-per-million (CPM) reads for each transcript across all samples, the log-odds ratio (LR), p-value and the false discovery rate (FDR).

| Gene               | D1       | D3       | D8       | Log CPM  | LR       | P-value  | FDR      |
|--------------------|----------|----------|----------|----------|----------|----------|----------|
| ENSCINT00000016852 | 3.098325 | 1.937186 | 2.566742 | 4.563039 | 46.46672 | 4.51E-10 | 5.68E-06 |
| ENSCINT00000035428 | -3.22002 | -1.22131 | -2.46122 | 7.020975 | 40.75257 | 7.38E-09 | 3.23E-05 |
| ENSCINT00000002977 | -1.53013 | -1.0677  | -1.47379 | 6.224487 | 40.66175 | 7.71E-09 | 3.23E-05 |
| ENSCINT00000032608 | 4.557647 | 3.535979 | 4.235177 | 6.21688  | 39.75887 | 1.20E-08 | 3.55E-05 |
| ENSCINT00000002984 | -1.50423 | -1.08892 | -1.44112 | 6.401095 | 39.42219 | 1.41E-08 | 3.55E-05 |
| ENSCINT00000032868 | 2.262125 | 1.583548 | 1.93285  | 2.6019   | 38.59793 | 2.11E-08 | 4.27E-05 |
| ENSCINT00000027705 | 1.731992 | -0.15224 | 0.908088 | 4.09522  | 38.35721 | 2.37E-08 | 4.27E-05 |
| ENSCINT00000007073 | 0.327442 | 0.854928 | 2.014151 | 2.34406  | 36.13358 | 7.02E-08 | 0.00011  |
| ENSCINT00000024202 | 1.474018 | 1.225616 | 1.445381 | 5.833982 | 35.47177 | 9.68E-08 | 0.000135 |
| ENSCINT00000033138 | 1.7482   | 1.311435 | 1.742597 | 3.809415 | 34.46096 | 1.58E-07 | 0.000164 |
| ENSCINT00000026775 | -1.28973 | -1.21463 | -1.13189 | 4.520945 | 34.35064 | 1.67E-07 | 0.000164 |
| ENSCINT00000004456 | 1.512945 | 1.743033 | 1.778986 | 5.989089 | 34.32915 | 1.69E-07 | 0.000164 |
| ENSCINT00000035694 | 2.309954 | 1.102321 | 1.762378 | 6.434744 | 34.32098 | 1.69E-07 | 0.000164 |
| ENSCINT00000025592 | 3.017282 | 3.123425 | 3.245969 | 6.504631 | 34.00433 | 1.98E-07 | 0.000167 |
| ENSCINT00000006259 | 3.332571 | 2.531958 | 3.310384 | 3.505102 | 33.99024 | 1.99E-07 | 0.000167 |
| ENSCINT00000020167 | 2.17282  | 0.332545 | 1.490045 | 5.017545 | 33.50138 | 2.52E-07 | 0.000189 |
| ENSCINT00000001716 | 2.312717 | 1.111006 | 1.758339 | 6.638359 | 33.47604 | 2.56E-07 | 0.000189 |
| ENSCINT00000011899 | -1.71796 | -0.94441 | -2.10835 | 3.457402 | 32.83697 | 3.49E-07 | 0.000244 |
| ENSCINT00000032994 | -2.69425 | 0.160872 | -1.97007 | 3.979899 | 32.70196 | 3.72E-07 | 0.000246 |
| ENSCINT00000025361 | 2.212304 | 1.594899 | 1.846057 | 4.300401 | 32.34783 | 4.42E-07 | 0.000278 |
| ENSCINT00000028348 | 3.429129 | 2.462152 | 3.326549 | 3.785931 | 32.13288 | 4.91E-07 | 0.000294 |
| ENSCINT00000026108 | 1.754231 | 1.061725 | 1.180144 | 3.182228 | 31.93871 | 5.39E-07 | 0.000307 |
| ENSCINT00000035931 | -0.28158 | 1.179899 | 1.595882 | 2.184825 | 31.85794 | 5.61E-07 | 0.000307 |
| ENSCINT00000011757 | -6.36496 | -1.24684 | -7.6126  | 9.727747 | 31.74412 | 5.93E-07 | 0.000311 |
| ENSCINT00000008590 | 2.467382 | 1.569956 | 2.535151 | 6.708561 | 31.36196 | 7.13E-07 | 0.000359 |
| ENSCINT00000032985 | -0.86054 | 1.008773 | -0.78458 | 3.356228 | 31.14362 | 7.93E-07 | 0.000384 |
| ENSCINT00000032844 | -0.53538 | 1.041566 | -0.45743 | 5.045268 | 30.78601 | 9.43E-07 | 0.000439 |
| ENSCINT00000035944 | -1.38717 | -1.07885 | -1.70512 | 5.903841 | 30.6048  | 1.03E-06 | 0.000461 |
| ENSCINT00000032350 | 1.785621 | 1.282163 | 1.676427 | 6.684467 | 30.53824 | 1.06E-06 | 0.000461 |
| ENSCINT00000019098 | 3.559869 | 3.728223 | 5.405249 | 7.644471 | 29.71462 | 1.58E-06 | 0.000661 |
| ENSCINT00000030148 | -0.3081  | 4.535797 | 0.998483 | 0.813906 | 29.61528 | 1.66E-06 | 0.000661 |
| ENSCINT00000027938 | 3.054621 | 3.005588 | 3.146558 | 4.915873 | 29.54031 | 1.72E-06 | 0.000661 |
| ENSCINT00000036027 | 4.338352 | 3.269428 | 4.350666 | 7.32871  | 29.52909 | 1.73E-06 | 0.000661 |
| ENSCINT00000031188 | 1.905082 | 1.590168 | 1.891427 | 5.606329 | 29.45779 | 1.79E-06 | 0.000664 |
| ENSCINT00000022223 | -1.49042 | -0.91746 | -1.82342 | 5.32221  | 29.30072 | 1.94E-06 | 0.000696 |
| ENSCINT00000011487 | -2.05306 | -1.32499 | -2.56398 | 7.981958 | 29.10234 | 2.13E-06 | 0.000745 |
| ENSCINT00000032225 | 2.305297 | 1.612717 | 2.254848 | 4.523618 | 29.008   | 2.23E-06 | 0.000758 |
| ENSCINT00000002481 | 2.19177  | 1.552399 | 2.314943 | 6.738536 | 28.90293 | 2.35E-06 | 0.000777 |
| ENSCINT00000000568 | -1.50212 | -0.25641 | -2.51532 | 6.335878 | 28.78391 | 2.49E-06 | 0.000802 |
| ENSCINT00000028559 | 2.597754 | 2.352515 | 2.495206 | 4.040942 | 28.71667 | 2.57E-06 | 0.000808 |

|                    |          |          |          |          |          |          |          |
|--------------------|----------|----------|----------|----------|----------|----------|----------|
| ENSCINT00000003420 | 3.562484 | 3.726827 | 5.392754 | 7.796918 | 28.52496 | 2.82E-06 | 0.000845 |
| ENSCINT00000025489 | 0.770184 | 1.443693 | 1.503457 | 5.487297 | 28.49499 | 2.86E-06 | 0.000845 |
| ENSCINT00000033273 | 1.916998 | 1.028707 | 0.953415 | 3.458381 | 28.4736  | 2.89E-06 | 0.000845 |
| ENSCINT00000033223 | 0.636257 | 1.753739 | -0.12438 | 3.275393 | 28.2369  | 3.24E-06 | 0.000926 |
| ENSCINT00000025362 | 1.951318 | 1.250685 | 1.582079 | 3.297809 | 27.95591 | 3.71E-06 | 0.001002 |
| ENSCINT00000031265 | 2.989742 | 3.336663 | 3.300771 | 5.983266 | 27.93805 | 3.74E-06 | 0.001002 |
| ENSCINT00000004784 | 2.275759 | 2.238537 | 2.466577 | 5.044132 | 27.78762 | 4.02E-06 | 0.001055 |
| ENSCINT00000013223 | 1.852826 | 0.756334 | 1.732808 | 4.144229 | 27.52185 | 4.58E-06 | 0.001175 |
| ENSCINT00000024974 | -1.48981 | -0.89557 | -1.43528 | 4.697763 | 27.27595 | 5.15E-06 | 0.001265 |
| ENSCINT00000013341 | 3.758532 | 3.522847 | 3.186755 | 2.681757 | 27.24511 | 5.23E-06 | 0.001265 |
| ENSCINT00000032086 | 0.721692 | -0.01242 | 1.038339 | 5.501273 | 26.97714 | 5.95E-06 | 0.001413 |
| ENSCINT00000026055 | 1.852519 | 1.077507 | 1.567328 | 4.766345 | 26.84658 | 6.34E-06 | 0.001477 |
| ENSCINT00000035303 | 2.353525 | 1.833407 | 2.131559 | 6.94355  | 26.62773 | 7.05E-06 | 0.0016   |
| ENSCINT00000008989 | 1.872759 | 1.571683 | 2.227709 | 3.117162 | 26.59862 | 7.15E-06 | 0.0016   |
| ENSCINT00000024522 | -1.46791 | -0.57752 | -0.63521 | 5.609243 | 26.56846 | 7.25E-06 | 0.0016   |
| ENSCINT00000028150 | -2.49933 | -0.30613 | -0.55287 | 1.952476 | 26.45812 | 7.65E-06 | 0.001658 |
| ENSCINT00000030610 | 1.024364 | 1.553978 | 0.409597 | 3.394669 | 26.31288 | 8.20E-06 | 0.001737 |
| ENSCINT00000036569 | -2.2097  | -1.24172 | -1.90682 | 4.971763 | 26.29201 | 8.28E-06 | 0.001737 |
| ENSCINT00000032652 | 1.977173 | 1.221444 | 0.795163 | 4.687042 | 26.25809 | 8.42E-06 | 0.001737 |
| ENSCINT00000000054 | 1.395189 | 0.911731 | 1.078716 | 5.495732 | 26.1318  | 8.95E-06 | 0.001816 |
| ENSCINT00000033595 | 1.880168 | 1.288566 | 1.386992 | 3.66374  | 25.99658 | 9.55E-06 | 0.001907 |
| ENSCINT00000014006 | -1.27431 | -1.04256 | -1.71716 | 5.775915 | 25.9273  | 9.88E-06 | 0.001941 |
| ENSCINT00000026214 | 2.028277 | 1.422108 | 1.651265 | 7.230824 | 25.8628  | 1.02E-05 | 0.001962 |
| ENSCINT00000014412 | 1.51661  | 1.226968 | 1.78477  | 6.033267 | 25.84125 | 1.03E-05 | 0.001962 |
| ENSCINT00000036350 | 1.606366 | 0.708197 | 1.395413 | 6.248858 | 25.49822 | 1.21E-05 | 0.002247 |
| ENSCINT00000026747 | -1.22634 | -0.83818 | -1.14972 | 3.734346 | 25.26226 | 1.36E-05 | 0.002481 |
| ENSCINT00000035153 | 1.878089 | 1.61227  | 1.915729 | 6.052242 | 25.20252 | 1.40E-05 | 0.002517 |
| ENSCINT00000030493 | 1.880723 | 1.339447 | 1.82329  | 5.890483 | 25.0873  | 1.48E-05 | 0.002592 |
| ENSCINT00000003632 | -1.04793 | -0.22791 | -1.02722 | 5.139684 | 25.08275 | 1.48E-05 | 0.002592 |
| ENSCINT00000027151 | 1.453924 | 0.682049 | 1.770972 | 4.751986 | 24.79404 | 1.70E-05 | 0.002898 |
| ENSCINT00000026302 | -1.58108 | -1.24707 | -1.34202 | 3.126248 | 24.73829 | 1.75E-05 | 0.002926 |
| ENSCINT00000035594 | 1.299936 | 1.311219 | 0.600321 | 4.578336 | 24.71861 | 1.77E-05 | 0.002926 |
| ENSCINT00000017186 | 1.540691 | 0.979251 | 1.575683 | 5.587028 | 24.509   | 1.96E-05 | 0.003195 |
| ENSCINT00000033079 | 2.628704 | 3.080833 | 2.944594 | 4.871562 | 24.45475 | 2.01E-05 | 0.003237 |
| ENSCINT00000019180 | -1.26813 | -0.83277 | -2.37976 | 6.432859 | 24.41501 | 2.05E-05 | 0.003258 |
| ENSCINT00000019977 | -1.6813  | -1.12302 | -1.99148 | 8.0157   | 24.36215 | 2.10E-05 | 0.0033   |
| ENSCINT00000003802 | 2.284735 | 1.542614 | 2.341006 | 7.0765   | 24.287   | 2.18E-05 | 0.003379 |
| ENSCINT00000003531 | 1.654603 | 1.465221 | 2.099448 | 2.608603 | 24.18119 | 2.29E-05 | 0.003512 |
| ENSCINT00000028739 | 1.935536 | 1.926145 | 2.013343 | 2.574675 | 24.10486 | 2.38E-05 | 0.003558 |
| ENSCINT00000014408 | -0.8781  | 0.263452 | -1.27932 | 7.501916 | 24.10435 | 2.38E-05 | 0.003558 |
| ENSCINT00000015921 | -1.18216 | -0.1243  | -1.92346 | 9.029778 | 24.04414 | 2.45E-05 | 0.003607 |



|                    |          |          |          |          |          |          |          |
|--------------------|----------|----------|----------|----------|----------|----------|----------|
| ENSCINT00000026146 | 1.708729 | 1.024801 | 0.960141 | 4.078188 | 24.02666 | 2.47E-05 | 0.003607 |
| ENSCINT00000019790 | -1.35198 | -0.81971 | -1.04304 | 4.47655  | 23.65833 | 2.94E-05 | 0.004172 |
| ENSCINT00000016537 | -1.15233 | -0.59347 | -1.90731 | 5.261657 | 23.65245 | 2.95E-05 | 0.004172 |
| ENSCINT00000007608 | -0.8188  | 1.266185 | -1.40594 | 3.77316  | 23.60267 | 3.02E-05 | 0.004226 |
| ENSCINT00000026781 | 2.126312 | 2.857093 | 2.49941  | 2.230104 | 23.52044 | 3.15E-05 | 0.004332 |
| ENSCINT00000030474 | 2.633322 | 1.555422 | 2.481196 | 3.036695 | 23.47739 | 3.21E-05 | 0.004332 |
| ENSCINT00000014954 | 0.59938  | 1.384436 | 1.155239 | 5.007486 | 23.45115 | 3.25E-05 | 0.004332 |
| ENSCINT00000033632 | -0.66405 | 0.617989 | -0.49441 | 3.629328 | 23.43849 | 3.27E-05 | 0.004332 |
| ENSCINT00000034741 | -0.82072 | 0.711306 | -1.46228 | 4.155282 | 23.35469 | 3.41E-05 | 0.004463 |
| ENSCINT00000034412 | 1.204013 | 0.03391  | 0.174057 | 4.080249 | 23.14652 | 3.76E-05 | 0.004844 |
| ENSCINT00000032867 | -1.57153 | 0.226418 | -0.24336 | 2.905456 | 23.14102 | 3.77E-05 | 0.004844 |
| ENSCINT00000034646 | 0.943009 | -0.13803 | 0.813668 | 4.121404 | 22.96988 | 4.10E-05 | 0.005141 |
| ENSCINT00000017459 | 2.845555 | 2.293428 | 2.970008 | 3.926828 | 22.95417 | 4.13E-05 | 0.005141 |
| ENSCINT00000018897 | -1.03046 | -0.66948 | -1.68872 | 6.223468 | 22.88748 | 4.26E-05 | 0.005256 |
| ENSCINT00000031597 | 2.110332 | 2.26267  | 1.897063 | 5.360081 | 22.6928  | 4.68E-05 | 0.005715 |
| ENSCINT00000015837 | 1.428457 | 1.019796 | 1.594715 | 6.861986 | 22.51865 | 5.09E-05 | 0.006153 |
| ENSCINT00000031769 | -0.3514  | 1.159585 | -0.57168 | 8.421046 | 22.44809 | 5.26E-05 | 0.006304 |
| ENSCINT00000029107 | -0.97639 | 0.141701 | -1.84955 | 7.122314 | 22.39106 | 5.41E-05 | 0.006418 |
| ENSCINT00000036347 | -0.17579 | 1.573782 | 2.180908 | 2.574863 | 22.35321 | 5.51E-05 | 0.006445 |
| ENSCINT00000030882 | -1.99138 | -0.6003  | -1.94243 | 5.642182 | 22.34338 | 5.53E-05 | 0.006445 |
| ENSCINT00000035546 | -1.06794 | -0.51645 | -1.44097 | 5.183871 | 22.17655 | 5.99E-05 | 0.006917 |
| ENSCINT00000015866 | -1.68144 | -0.94476 | -1.04493 | 6.167284 | 22.12632 | 6.14E-05 | 0.007019 |
| ENSCINT00000030348 | 2.548801 | 1.458251 | 2.977134 | 2.373254 | 22.10806 | 6.19E-05 | 0.007019 |
| ENSCINT00000002897 | 1.402095 | 0.754612 | 1.248309 | 7.101335 | 21.96245 | 6.64E-05 | 0.007459 |
| ENSCINT00000032583 | -1.73443 | -1.09495 | -1.68132 | 4.365313 | 21.93037 | 6.74E-05 | 0.007499 |
| ENSCINT00000034609 | 1.827809 | 0.454761 | 1.171696 | 5.189039 | 21.89777 | 6.85E-05 | 0.007499 |
| ENSCINT00000027606 | -1.6392  | -0.06996 | -2.59095 | 5.844567 | 21.89622 | 6.86E-05 | 0.007499 |
| ENSCINT00000023044 | -0.95917 | -0.60367 | -1.64735 | 6.081949 | 21.8083  | 7.15E-05 | 0.007677 |
| ENSCINT00000029051 | 1.494676 | 0.664327 | 1.270528 | 4.261694 | 21.78083 | 7.25E-05 | 0.007677 |
| ENSCINT00000033422 | 1.038958 | 1.266556 | 1.854636 | 5.080862 | 21.77638 | 7.26E-05 | 0.007677 |
| ENSCINT00000021573 | -1.45784 | -1.67054 | -2.95152 | 2.942052 | 21.75519 | 7.33E-05 | 0.007677 |
| ENSCINT00000032176 | -1.50772 | -1.49476 | -1.968   | 7.707606 | 21.74881 | 7.36E-05 | 0.007677 |
| ENSCINT00000005981 | -1.342   | -1.10509 | -1.09751 | 5.142449 | 21.74109 | 7.38E-05 | 0.007677 |
| ENSCINT00000021540 | 1.62201  | 0.641764 | 1.573684 | 3.005147 | 21.67397 | 7.63E-05 | 0.007818 |
| ENSCINT00000031929 | -1.29725 | -0.76907 | -1.02882 | 4.710438 | 21.66629 | 7.65E-05 | 0.007818 |
| ENSCINT00000035165 | 1.676075 | 0.473725 | 1.212376 | 6.093736 | 21.65184 | 7.71E-05 | 0.007818 |
| ENSCINT00000026583 | -1.8464  | -1.01721 | -2.30772 | 6.415947 | 21.58159 | 7.97E-05 | 0.008021 |
| ENSCINT00000018262 | 1.346291 | 1.139975 | 1.667191 | 4.805085 | 21.51924 | 8.21E-05 | 0.008198 |
| ENSCINT00000006770 | -0.80847 | -0.60223 | -1.34262 | 5.853285 | 21.38488 | 8.76E-05 | 0.008674 |
| ENSCINT00000035966 | -1.01791 | -1.06917 | -1.41617 | 2.725601 | 21.15996 | 9.75E-05 | 0.00953  |
| ENSCINT00000023490 | -1.58469 | -1.29439 | -2.48329 | 2.919561 | 21.14377 | 9.83E-05 | 0.00953  |

|                    |          |          |          |          |          |          |          |
|--------------------|----------|----------|----------|----------|----------|----------|----------|
| ENSCINT00000024102 | -0.51299 | 1.200259 | -0.33122 | 3.222734 | 21.13147 | 9.89E-05 | 0.00953  |
| ENSCINT00000014508 | 2.424984 | 2.44592  | 3.347098 | 4.588865 | 21.12339 | 9.92E-05 | 0.00953  |
| ENSCINT00000033573 | 1.880273 | 1.399154 | 1.664271 | 4.519183 | 21.08683 | 0.000101 | 0.009624 |
| ENSCINT00000011492 | 1.301991 | 1.288303 | 1.903647 | 3.967857 | 21.06722 | 0.000102 | 0.009642 |
| ENSCINT00000037150 | -1.3551  | -0.6877  | -1.37201 | 4.155905 | 21.03527 | 0.000104 | 0.009717 |
| ENSCINT00000003246 | -1.88405 | -0.98538 | -1.57729 | 5.588495 | 20.99508 | 0.000106 | 0.009832 |
| ENSCINT00000020067 | -1.94314 | -1.48598 | -2.12918 | 6.062966 | 20.97717 | 0.000106 | 0.009844 |
| ENSCINT00000033135 | 2.490077 | 1.878289 | 2.48235  | 5.438765 | 20.95103 | 0.000108 | 0.009895 |
| ENSCINT00000035350 | -1.19525 | -0.73441 | -1.08726 | 4.802563 | 20.88986 | 0.000111 | 0.010062 |
| ENSCINT00000019588 | -0.93234 | -0.2213  | -1.81912 | 7.161376 | 20.88583 | 0.000111 | 0.010062 |
| ENSCINT00000036413 | 1.256396 | 2.005865 | 1.917103 | 7.555305 | 20.77812 | 0.000117 | 0.010474 |
| ENSCINT00000037147 | 1.618273 | 1.476749 | 1.646818 | 1.999325 | 20.772   | 0.000117 | 0.010474 |
| ENSCINT00000028768 | 2.43727  | 2.830234 | 3.244211 | 1.214934 | 20.73452 | 0.00012  | 0.010588 |
| ENSCINT00000036828 | 0.269046 | 2.98285  | 1.07999  | 0.442566 | 20.66042 | 0.000124 | 0.01084  |
| ENSCINT00000007024 | -1.11589 | -0.98167 | -1.39036 | 6.380049 | 20.65604 | 0.000124 | 0.01084  |
| ENSCINT00000010862 | 2.172854 | 1.791882 | 1.674204 | 7.495368 | 20.59464 | 0.000128 | 0.011068 |
| ENSCINT00000018141 | 1.589484 | 1.120402 | 2.369942 | 4.452461 | 20.58355 | 0.000128 | 0.011068 |
| ENSCINT00000012021 | -1.02839 | -0.19128 | -2.31158 | 5.330901 | 20.52316 | 0.000132 | 0.011315 |
| ENSCINT00000029222 | -0.8309  | -0.67938 | -1.70134 | 3.250884 | 20.49803 | 0.000134 | 0.01133  |
| ENSCINT00000023546 | 1.685425 | 1.459312 | 1.672494 | 3.366844 | 20.47795 | 0.000135 | 0.01133  |
| ENSCINT00000034280 | 1.933934 | 1.600525 | 2.063839 | 6.803917 | 20.42018 | 0.000139 | 0.01157  |
| ENSCINT00000013119 | -1.7649  | -1.13599 | -2.12581 | 8.184818 | 20.39249 | 0.000141 | 0.011647 |
| ENSCINT00000032988 | -1.5464  | -0.70509 | -1.89    | 4.96977  | 20.37222 | 0.000142 | 0.011684 |
| ENSCINT00000023028 | 1.847412 | 1.427829 | 1.699159 | 3.095845 | 20.30671 | 0.000147 | 0.011807 |
| ENSCINT00000035141 | 0.42601  | 2.240434 | 2.749661 | 1.444743 | 20.29729 | 0.000147 | 0.011807 |
| ENSCINT00000010442 | -1.14094 | 0.187256 | -1.23458 | 6.672694 | 20.29608 | 0.000147 | 0.011807 |
| ENSCINT00000000708 | 1.806198 | 1.320377 | 1.6982   | 4.29465  | 20.24783 | 0.000151 | 0.012006 |
| ENSCINT00000037260 | 4.036479 | 0.737766 | 3.764286 | 1.108775 | 20.21124 | 0.000153 | 0.012141 |
| ENSCINT00000007645 | 0.960047 | 0.406747 | 1.35713  | 4.106965 | 20.16915 | 0.000157 | 0.012235 |
| ENSCINT00000003840 | -0.50788 | 0.242541 | -1.25624 | 6.245288 | 20.16895 | 0.000157 | 0.012235 |
| ENSCINT00000022115 | 2.796538 | 2.052252 | 2.853218 | 3.326468 | 20.07628 | 0.000164 | 0.012627 |
| ENSCINT00000000095 | -0.94852 | -0.85692 | -1.07528 | 4.857012 | 20.06409 | 0.000165 | 0.012627 |
| ENSCINT00000011603 | 1.441458 | 0.875331 | 1.338376 | 6.635576 | 20.03681 | 0.000167 | 0.012715 |
| ENSCINT00000030512 | 1.858929 | 1.190003 | 2.035351 | 6.906521 | 19.96688 | 0.000172 | 0.013055 |
| ENSCINT00000022097 | -0.87266 | -1.06565 | -1.25262 | 5.426487 | 19.95622 | 0.000173 | 0.013055 |
| ENSCINT00000026050 | -1.21694 | -0.83919 | -1.37333 | 3.303373 | 19.90425 | 0.000178 | 0.013304 |
| ENSCINT00000017324 | 0.788123 | -0.39718 | 0.822352 | 7.837974 | 19.85649 | 0.000182 | 0.013524 |
| ENSCINT00000035419 | -1.01094 | -0.87682 | -0.21149 | 5.346584 | 19.84501 | 0.000183 | 0.013524 |
| ENSCINT00000033419 | -1.42958 | -0.18352 | -1.28467 | 2.880211 | 19.75831 | 0.00019  | 0.013951 |
| ENSCINT00000014406 | -0.78461 | 0.52097  | -1.04012 | 8.083646 | 19.71414 | 0.000195 | 0.014136 |
| ENSCINT00000030616 | -0.58379 | -0.23779 | -1.2022  | 4.926494 | 19.70349 | 0.000196 | 0.014136 |

|                    |          |          |          |          |          |          |          |
|--------------------|----------|----------|----------|----------|----------|----------|----------|
| ENSCINT00000026237 | -1.66355 | -1.03356 | -1.12379 | 6.102603 | 19.68916 | 0.000197 | 0.014151 |
| ENSCINT00000026510 | -0.3815  | -1.55021 | -1.3728  | 5.581832 | 19.6382  | 0.000202 | 0.014417 |
| ENSCINT00000011017 | 0.992856 | 1.241105 | 1.302014 | 4.751662 | 19.61393 | 0.000204 | 0.014502 |
| ENSCINT00000032809 | 2.136538 | 1.472002 | 2.165598 | 2.273211 | 19.50658 | 0.000215 | 0.014981 |
| ENSCINT00000024573 | -0.22809 | 0.634049 | 1.021972 | 4.540176 | 19.49695 | 0.000216 | 0.014981 |
| ENSCINT00000014727 | -1.15388 | -0.91662 | -1.05892 | 4.437844 | 19.48734 | 0.000217 | 0.014981 |
| ENSCINT00000033441 | 0.702089 | 2.041806 | 2.614889 | 1.628717 | 19.43178 | 0.000223 | 0.015199 |
| ENSCINT00000012563 | -1.06766 | -0.53258 | -1.05038 | 6.270015 | 19.42768 | 0.000223 | 0.015199 |
| ENSCINT00000011466 | 0.205543 | 1.201934 | 0.249328 | 5.27035  | 19.42269 | 0.000224 | 0.015199 |
| ENSCINT00000035711 | -0.65971 | 3.96077  | 1.781399 | -0.85441 | 19.39955 | 0.000226 | 0.015274 |
| ENSCINT00000030560 | -0.25014 | -0.60657 | 0.564694 | 5.276593 | 19.36394 | 0.00023  | 0.015382 |
| ENSCINT00000035526 | 1.148724 | 1.648545 | 1.81382  | 3.918975 | 19.23812 | 0.000244 | 0.016002 |
| ENSCINT00000034599 | -0.60042 | 2.392886 | 0.54276  | 0.634363 | 19.23678 | 0.000244 | 0.016002 |
| ENSCINT00000017159 | 1.517057 | 1.233438 | 1.685588 | 7.15656  | 19.20361 | 0.000248 | 0.016172 |
| ENSCINT00000012374 | 0.406242 | 1.199332 | 1.607309 | 3.795559 | 19.10618 | 0.00026  | 0.016802 |
| ENSCINT00000034946 | 1.462483 | 0.497555 | 1.084357 | 7.551393 | 19.10183 | 0.00026  | 0.016802 |
| ENSCINT00000030377 | 0.2984   | 2.318307 | -1.14541 | -0.47046 | 19.08712 | 0.000262 | 0.016833 |
| ENSCINT00000030216 | -1.14705 | -0.61098 | -1.51509 | 3.826263 | 18.84827 | 0.000294 | 0.01867  |
| ENSCINT00000008836 | -0.83621 | -0.76004 | -1.27827 | 6.440179 | 18.82874 | 0.000297 | 0.01875  |
| ENSCINT00000031563 | -1.1371  | -0.60401 | -1.32364 | 5.697027 | 18.75348 | 0.000307 | 0.01915  |
| ENSCINT00000002707 | 1.879027 | 1.051374 | 1.643747 | 8.495753 | 18.75288 | 0.000308 | 0.01915  |
| ENSCINT00000015829 | -1.47365 | -1.4383  | -1.81888 | 7.741569 | 18.69832 | 0.000316 | 0.019557 |
| ENSCINT00000009260 | -0.79015 | -0.90684 | -1.04533 | 4.675848 | 18.58697 | 0.000333 | 0.020237 |
| ENSCINT00000007710 | 0.944562 | 0.209932 | 0.833729 | 6.164744 | 18.58539 | 0.000333 | 0.020237 |
| ENSCINT00000019109 | -1.67995 | -1.2994  | -1.91244 | 6.970733 | 18.55537 | 0.000338 | 0.020402 |
| ENSCINT00000031891 | -1.01583 | -0.62954 | -1.40337 | 6.274261 | 18.52148 | 0.000343 | 0.020564 |
| ENSCINT00000031438 | -2.15656 | -0.93647 | -0.95388 | 2.214881 | 18.497   | 0.000347 | 0.020706 |
| ENSCINT00000023829 | -1.42662 | -0.69912 | -1.53927 | 6.799656 | 18.38175 | 0.000367 | 0.021667 |
| ENSCINT00000030380 | 0.670521 | 2.163038 | 2.761923 | 1.783421 | 18.31472 | 0.000379 | 0.022058 |
| ENSCINT00000034097 | -1.28013 | -0.51256 | -1.07639 | 6.169759 | 18.29437 | 0.000382 | 0.02217  |
| ENSCINT00000031399 | 1.304125 | 2.388119 | 1.810823 | 1.892024 | 18.26872 | 0.000387 | 0.022338 |
| ENSCINT00000007133 | -0.93008 | -0.70762 | -1.31866 | 3.687896 | 18.20357 | 0.000399 | 0.022746 |
| ENSCINT00000007938 | -1.08791 | 0.144359 | -1.05668 | 8.332393 | 18.19458 | 0.000401 | 0.022746 |
| ENSCINT00000009107 | -0.59773 | -0.74216 | -1.23733 | 5.926732 | 18.1924  | 0.000401 | 0.022746 |
| ENSCINT00000002830 | -1.03627 | -0.63064 | -0.96203 | 5.607682 | 18.16489 | 0.000407 | 0.022942 |
| ENSCINT00000035368 | -1.78333 | -0.61675 | -1.44221 | 2.313764 | 18.11228 | 0.000417 | 0.023313 |
| ENSCINT00000015400 | 1.114144 | 0.461821 | 1.402466 | 3.454253 | 18.09742 | 0.00042  | 0.023375 |
| ENSCINT00000015426 | -1.83488 | -0.40451 | -2.28688 | 9.181042 | 18.0154  | 0.000437 | 0.02409  |
| ENSCINT00000030439 | -1.03924 | -1.11877 | -0.8353  | 4.88893  | 17.98258 | 0.000444 | 0.024362 |
| ENSCINT00000013593 | 1.362078 | 0.541082 | 1.050579 | 4.61297  | 17.9403  | 0.000452 | 0.02464  |
| ENSCINT00000007799 | 1.360733 | 0.65885  | 1.296124 | 7.173495 | 17.91233 | 0.000459 | 0.024756 |

|                    |          |          |          |          |          |          |          |
|--------------------|----------|----------|----------|----------|----------|----------|----------|
| ENSCINT00000025302 | -1.34302 | -0.93516 | -1.25686 | 4.084346 | 17.90189 | 0.000461 | 0.024772 |
| ENSCINT00000035652 | 1.159335 | 0.426684 | 1.046279 | 3.546009 | 17.85664 | 0.000471 | 0.024988 |
| ENSCINT00000012587 | 2.268867 | 1.676089 | 2.167155 | 9.811438 | 17.85259 | 0.000472 | 0.024988 |
| ENSCINT00000033254 | 2.435564 | 1.645713 | 2.737266 | 1.882748 | 17.84316 | 0.000474 | 0.024988 |
| ENSCINT00000016646 | -1.44234 | -0.89171 | -1.16823 | 3.920578 | 17.78538 | 0.000487 | 0.025526 |
| ENSCINT00000008248 | 1.263465 | 0.629972 | 0.984248 | 3.715625 | 17.71898 | 0.000503 | 0.026126 |
| ENSCINT00000021972 | 1.204312 | 0.690657 | 2.135922 | 2.302804 | 17.7076  | 0.000505 | 0.026159 |
| ENSCINT00000036255 | 1.606733 | 1.28778  | 1.465397 | 7.230524 | 17.6071  | 0.00053  | 0.027324 |
| ENSCINT00000036109 | -1.43273 | -1.56692 | -1.45097 | 2.073842 | 17.50906 | 0.000555 | 0.02831  |
| ENSCINT00000013369 | -1.21375 | -1.06448 | -0.78386 | 3.180608 | 17.42466 | 0.000578 | 0.029196 |
| ENSCINT00000024647 | -0.67587 | -0.38089 | -1.26045 | 5.860513 | 17.25588 | 0.000626 | 0.031005 |
| ENSCINT00000010557 | 1.721324 | 1.957581 | 2.657829 | 8.815755 | 17.18312 | 0.000648 | 0.031595 |
| ENSCINT00000033284 | -0.84007 | -0.62179 | -1.26088 | 5.778297 | 17.14078 | 0.000661 | 0.032111 |
| ENSCINT00000026912 | 0.953367 | 0.099722 | 0.319551 | 6.029536 | 17.06016 | 0.000687 | 0.032979 |
| ENSCINT00000020911 | -1.14308 | -0.79989 | -0.79303 | 5.653056 | 16.9951  | 0.000708 | 0.033881 |
| ENSCINT00000015475 | 1.793453 | 1.288797 | 1.778298 | 8.694303 | 16.97947 | 0.000714 | 0.034004 |
| ENSCINT00000022294 | -1.16622 | -0.93811 | -1.20889 | 3.404193 | 16.95715 | 0.000721 | 0.034235 |
| ENSCINT00000019728 | 1.025421 | 0.309665 | 0.596331 | 4.855044 | 16.89611 | 0.000742 | 0.034791 |
| ENSCINT00000026049 | -1.03897 | -0.66854 | -1.25922 | 3.156365 | 16.8915  | 0.000744 | 0.034791 |
| ENSCINT00000030392 | -1.91602 | -0.53935 | 0.07458  | 1.64221  | 16.72436 | 0.000805 | 0.036833 |
| ENSCINT00000030300 | 0.514693 | 0.92814  | 0.883444 | 4.445491 | 16.70885 | 0.000811 | 0.03691  |
| ENSCINT00000036269 | -1.0751  | -0.72339 | -1.38126 | 2.410628 | 16.70466 | 0.000813 | 0.03691  |
| ENSCINT00000012097 | -0.23593 | 0.356981 | -0.71218 | 5.805129 | 16.69083 | 0.000818 | 0.037018 |
| ENSCINT00000022871 | 1.756125 | 1.066405 | 1.484252 | 7.239002 | 16.61265 | 0.000849 | 0.038139 |
| ENSCINT00000000221 | 1.757283 | 1.06578  | 1.484273 | 7.237701 | 16.59546 | 0.000856 | 0.038313 |
| ENSCINT00000013976 | 1.41175  | 1.106735 | 0.431925 | 8.175381 | 16.58351 | 0.000861 | 0.038378 |
| ENSCINT00000002440 | 1.184075 | 0.505598 | 1.082442 | 6.95043  | 16.57688 | 0.000863 | 0.038378 |
| ENSCINT00000033773 | 1.757365 | 1.06652  | 1.477606 | 7.245335 | 16.50852 | 0.000892 | 0.039002 |
| ENSCINT00000036096 | 0.625128 | 0.526093 | 1.410228 | 2.590031 | 16.41012 | 0.000934 | 0.040329 |
| ENSCINT00000006610 | -0.63883 | -0.56977 | -1.20451 | 5.400503 | 16.40019 | 0.000939 | 0.040329 |
| ENSCINT00000036965 | -0.82918 | -0.63258 | -1.12796 | 4.310149 | 16.39504 | 0.000941 | 0.040329 |
| ENSCINT00000030479 | 0.983794 | 0.919293 | 1.383575 | 2.453036 | 16.39137 | 0.000943 | 0.040329 |
| ENSCINT00000014723 | -1.14652 | -0.95347 | -1.18338 | 3.424976 | 16.2416  | 0.001012 | 0.042284 |
| ENSCINT00000023320 | -1.57781 | -0.66803 | -1.84516 | 9.16051  | 16.24142 | 0.001012 | 0.042284 |
| ENSCINT00000016152 | -0.91094 | -0.01438 | -1.27018 | 8.475995 | 16.21921 | 0.001022 | 0.042572 |
| ENSCINT00000017961 | 1.757618 | 1.230161 | 1.955623 | 8.546694 | 16.213   | 0.001025 | 0.042572 |
| ENSCINT00000036964 | 2.123384 | 1.333847 | 2.089298 | 1.461417 | 16.0842  | 0.00109  | 0.044345 |
| ENSCINT00000012802 | -0.64633 | -0.35791 | -1.31389 | 2.658133 | 16.06299 | 0.001101 | 0.044345 |
| ENSCINT00000036234 | -1.3361  | -0.84091 | -1.38963 | 7.308478 | 16.06026 | 0.001102 | 0.044345 |
| ENSCINT00000019435 | -0.93934 | -0.50839 | -0.76884 | 5.462676 | 16.02827 | 0.001119 | 0.044826 |
| ENSCINT00000007510 | 0.615664 | 1.027976 | 1.280805 | 3.990421 | 15.99091 | 0.001139 | 0.045335 |
| ENSCINT00000024535 | 1.113495 | 0.483477 | 0.887441 | 5.747373 | 15.97185 | 0.001149 | 0.045445 |
| ENSCINT00000002493 | 1.108389 | 0.351535 | 1.033921 | 3.646435 | 15.8552  | 0.001214 | 0.046995 |
| ENSCINT00000037001 | 0.588361 | 0.618853 | 1.008867 | 5.160179 | 15.80646 | 0.001242 | 0.047503 |
| ENSCINT00000013284 | 1.072886 | 0.69822  | 1.282738 | 3.015824 | 15.74978 | 0.001276 | 0.048247 |



**Table S3. Concurrence of Differentially Expressed microRNAs Between Two Programs Relative to Day 0.** Results from EdgeR are shown after retaining only transcripts identified as differentially expressed by both EdgeR and DESeq2. Transcripts are indicated in the first column. Subsequent columns show the estimated  $\log_2$  fold-change (logFC) for each stage (D1 = one dpa, D3 = three dpa, D8 = eight dpa), the mean  $\log_2$  counts-per-million (CPM) reads for each transcript across all samples, the log-odds ratio (LR), p-value and the false discovery rate (FDR).

| miRNA            | D1       | D3       | D8       | Log CPM  | LR       | P-value  | FDR      |
|------------------|----------|----------|----------|----------|----------|----------|----------|
| miR-4009c-3p     | -0.33418 | -2.09444 | -2.52661 | 5.728668 | 48.61951 | 1.57E-10 | 4.39E-08 |
| 12_9033          | -2.77335 | 3.075175 | 2.830244 | 2.912204 | 40.4201  | 8.68E-09 | 1.21E-06 |
| miR-9-5p         | 6.949359 | 8.075647 | 7.575542 | 2.696617 | 29.0792  | 2.16E-06 | 0.0002   |
| miR-29-3p        | -1.28718 | -2.52153 | -2.26111 | 4.034371 | 27.0092  | 5.86E-06 | 0.000409 |
| HT000106.1_40026 | -1.49943 | -2.6622  | -4.57517 | 2.659776 | 22.53336 | 5.05E-05 | 0.002819 |
| miR-3598-5p      | -0.27293 | -1.36534 | -1.92305 | 16.23311 | 21.75303 | 7.34E-05 | 0.003414 |
| miR-219-5p       | 2.186326 | 3.027384 | 3.099589 | 6.114606 | 20.46434 | 0.000136 | 0.00542  |
| 3_16731          | -0.93918 | -1.82723 | -3.27397 | 3.00145  | 19.1393  | 0.000256 | 0.008923 |
| 7_23696          | 0.239673 | -3.11952 | -1.84066 | 1.849137 | 18.45138 | 0.000355 | 0.011003 |
| miR-200-3p       | -0.17735 | -0.94925 | -1.85287 | 9.98947  | 16.5221  | 0.000886 | 0.024722 |
| miR-133-3p       | 0.664604 | 1.540163 | 1.564872 | 13.12434 | 15.73898 | 0.001283 | 0.032532 |
| miR-4065-5p      | -0.17257 | -0.08662 | -1.4625  | 6.926986 | 15.03078 | 0.001791 | 0.041326 |
| HT000888.1_32283 | -0.47259 | -1.22849 | 0.616814 | 4.307231 | 14.86968 | 0.001931 | 0.041326 |
| miR-33           | -0.68271 | -2.45744 | -2.58391 | 1.761717 | 14.71853 | 0.002074 | 0.041326 |

**Table S4. Most Significantly Differentially Expressed Transcripts at 3 days post-amputation Compared to a Previous Study.**

Supplementary Table 2 modified from Hamada et al. (2015) contains the 30 most significantly differentially expressed genes at 3 days post amputation relative to non-regenerating oral siphons detected by microarray. Two columns have been added to right of the previous columns. The first indicates the Ensembl transcript identifier best matching the corresponding KH gene model used in the previous study. The second column contains a “Y” if the Ensembl transcript was significantly differentially expressed relative to zero days post amputation in the current study.

| Probe ID  | Fold Change (Ratio) | Gene Model   | HS Best Hit ID | Gene Name   | Ensembl ID         | Significant |
|-----------|---------------------|--|----------------|---|--------------------|-------------|
| CIYS2041  | 76.5                | SPKH.C11.10039.v1.D                                  | NP_064448.1    | barH-like 1 homeobox protein  | ENSCINT00000029737 |             |
| CIYS17996 | 44.4                | KH.C5.345.v1.A.SL1-1                                 | NP_079065.2    | transmembrane protein 180   | ENSCINT00000023271 |             |
| CIYS691   | 31.6                | SPKH.L87.10003.v1.D                                  | NP_057330.2    | 17-beta-hydroxysteroid dehydrogenase 14   | ENSCINT00000024253 |             |
| CIYS18457 | 25.6                | KH.C5.524.v2.A.nonSL7-1                              | NP_067052.2    | netrin 4 precursor  | ENSCINT00000015201 |             |
| CIYS1815  | 23.4                | KH.C10.417.v1.A.SL1-1                                | NP_003216.1    | trefoil factor 1 precursor  | ENSCINT00000032198 | Y           |
| CIYS18332 | 18.2                | Fis_citb014p06_20                                    | NP_899195.1    | protein SEC13 homolog isoform 1   | ENSCINT00000005198 |             |
| CIYS19632 | 16.3                | Chromosome 5:<br>625,279-<br>626,193 reverse strand. | KH:HT000010.1  | Uncharacterized protein<br>[Source:UniProtKB/TrEMBL;Acc:H2XMW7]                 | ENSCINT00000035801 |             |
| CIYS15440 | 14.3                | Fis_cicl013b17_20                                    | XM_002131970   |   | ENSCINT00000033860 |             |
| CIYS6125  | 14.2                | KH.C3.316.v3.R.ND1-1                                 | NP_009043.1    | thrombospondin 3 precursor  | ENSCINT00000017560 |             |
| CIYS12078 | 13                  | KH.C9.21.v2.A.SL3-2                                  |                |   | ENSCINT00000016952 |             |
| CIYS12519 | 12.5                | KH.C14.177.v3.B.SL5-1                                | NP_002878.2    | arginyl-tRNA synthetase, cytoplasmic  | ENSCINT00000015003 |             |
| CIYS19591 | 12.1                | KH.C1.122.v1.R.ND1-1                                 |                |   | ENSCINT00000003964 |             |
| CIYS2437  | 11.8                | SPKH.C7.10126.v4.D                                   | NP_056344.2    | DBH-like monooxygenase protein 1 isoform 2                                      | ENSCINT00000033602 |             |
| CIYS3070  | 11.8                | KH.C10.417.v1.A.SL1-1                                | NP_003216.1    | trefoil factor 1 precursor  | ENSCINT00000034671 |             |
| CIYS14823 | 11.5                | KH.L100.2.v2.A.SL1-1                                 | NP_078918.3    | polypeptide N-acetylgalactosaminyltransferase 12                                | ENSCINT00000037096 | Y           |
| CIYS9653  | 10.8                | TC146939   |                |   | N/A                |             |
| CIYS18259 | 10.4                | KH.C12.235.v2.A.SL2-1                                |                | 1500 AA double-pass TM protein  | ENSCINT00000003412 |             |
| CIYS12181 | 10                  | KH.C8.253.v1.A.ND1-1                                 |                | Integrin alpha-2  | ENSCINT00000024577 |             |
| CIYS16388 | 9.8                 | Fis_cieg019m07_20                                    | NP_000311.2    | quinoid dihydropteridine reductase  | ENSCINT00000019999 | Y           |
| CIYS18283 | 9.2                 | KH.S597.1.v2.B.ND4-1                                 | NP_002254.2    | kinesin-like protein KIFC1  | ENSCINT00000001181 |             |
| CIYS2033  | 9.1                 | KH.C7.123.v1.A.SL1-1                                 | NP_060087.3    | notch1 preproprotein  | ENSCINT00000022796 | Y           |
| CIYS15068 | 9.1                 | KH.L6.1.v2.A.ND2-1                                   | NP_001035257.1 | beta-1,3-N-acetylglucosaminyltransferase lunatic fringe isoform a preproprotein | ENSCINT00000018757 |             |

|           |     |                         |             |   |                    |   |
|-----------|-----|-------------------------|-------------|---|--------------------|---|
| CIYS11893 | 8.9 | NA                      |             |   | N/A                |   |
| CIYS19123 | 8.8 | KH.C1.249.v1.A.ND1-1    | NP_060774.2 | proline-rich protein 11                     | ENSCINT00000013708 |   |
| CIYS12958 | 8.7 | KH.C4.504.v1.A.nonSL3-1 | NP_973732.1 | forkhead box protein M1 isoform 3           | ENSCINT00000017891 |   |
| CIYS2001  | 8.6 | SPKH.C3.10151.v2.D      | NP_002996.2 | selectin P precursor                        | N/A                |   |
| CIYS3649  | 8.2 | SPKH.L96.10023.v1.E     |             |   | N/A                |   |
| CIYS8857  | 8.1 | KH.L41.4.v1.A.ND1-1     | NP_060656.2 | DUF - hypothetical protein LOC55732         | ENSCINT00000001400 |   |
| CIYS9266  | 7.5 | KH.C1.1083.v1.A.SL1-1   | NP_004429.1 | ephrin receptor EphA4 precursor             | ENSCINT00000025459 | Y |
| CIYS13813 | 7.4 | TC146713                | NP_004781.2 | solute carrier family 22 member 6 isoform a | ENSCINT00000027773 |   |

**Table S5. Transcript Names and Primer Sequences Used in this Study.** All transcript names used in the primary text are listed here with the corresponding Ensembl transcript identifier, a description of the transcript and primer sequences used for qRT-PCR validation, if applicable.

| Name                   | Description                           | ID                 | Forward Primer        | Reverse Primer        |
|------------------------|---------------------------------------|--------------------|-----------------------|-----------------------|
| Caspase-2-like         | Caspase-2-like                        | ENSCINT00000002830 | ATGACGTGCTTGCATTGTTC  | CGACCCACCTCAGTAAGCAT  |
| FIBCD1a                | Fibrinogen C domain containing 1      | ENSCINT00000003420 | GAAACCGAACTGGTCGAAAG  | CCGGATACAGCAAGTGCATA  |
| Rev-erb                | Rev-erb                               | ENSCINT00000004784 | GTCGAATCCCAAAGAAGCAG  | GTGTTTCTTGCACCGTTTGA  |
| TNFR-associated        | TNF receptor-associated factor 3-like | ENSCINT00000005981 | ATGGGCTATGTTGGATGGAA  | CAATCTGCTGCTCAAATCCA  |
| Tolloid                | Tolloid                               | ENSCINT00000007799 | GTAAAGAAGCCGGGTGTGAG  | CTGTTGTATGCGAGGCAGAA  |
| HSP70                  | Heat shock protein 70                 | ENSCINT00000011757 | TGATAAACGAACCCACAGCA  | ATCCAACCTCGACAGCAGCTT |
| HB3                    | Non-symbiotic hemoglobin 3            | ENSCINT00000013341 | TGAGTAACGTTGGACTTGCTG | CCCAAGCTTGCATTACTGGT  |
| Tomoregulin            | Tomoregulin-1-like                    | ENSCINT00000016852 | TGCTTGGATGAAGTTGATGG  | CATGCGACTGTAACGATTCC  |
| Prospero               | Prospero homeobox protein             | ENSCINT00000018262 | GCACCTCAGCATTACCCAAT  | TTGGTCACGACGTCAAGAAA  |
| FIBCD1b                | Fibrinogen C domain containing 1      | ENSCINT00000019098 | GAAACCGAACTGGTCGAAAG  | CCGGATACAGCAAGTGCATA  |
| DIAP2                  | Drosophila Inhibitor of Apoptosis 2   | ENSCINT00000020067 | TTGCAAGCACCCATATACGA  | GATGTGGATGGTTTGGGAGT  |
| bZIP                   | CCAAT/Enhancer Binding Protein        | ENSCINT00000023320 | CGCTCGTACTCAAGCAACAG  | ACAACATCATGGGACGGATT  |
| TLR2                   | Toll-like receptor 2                  | ENSCINT00000024647 | CAGTGATTCCGATGATGTGG  | GGTGCTTGGATGGCAGTAAT  |
| TNFR                   | Tumor Necrosis Factor Receptor        | ENSCINT00000026302 | GAAGATGCGTCCCATGCTAT  | GAATGCCATGGACATCACAG  |
| NEK11-like             | NIMA related kinase 11-like           | ENSCINT00000026775 | GAATATTGTGAGGGCGGAGA  | ACAACACCAAGGGACCAAAG  |
| Matrillin              | VWF domain containing protein         | ENSCINT00000027938 | CGTAAAGGAATGGGTGAAGC  | TGAATGACATCCGGCAAGTA  |
| Laminin subunit beta 2 | EGF domain containing protein         | ENSCINT00000031265 | TTTCTTCTTTGGCGATGCTT  | TCAGCGCTTCTTCTCACGTA  |
| IGF-like               | Insulin-like 3 protein                | ENSCINT00000031399 | CTGGAACGAAGTGCAAAGGT  | TATTGCCATGCAGGTAACGA  |
| DBX1-A                 | Hlx Homeobox protein DBX1-A           | ENSCINT00000033135 | TCAGTCCAACCTATGCACCA  | AGGGTAAGATGGGTGTGACG  |
| Hsp90                  | Heat shock protein 90                 | ENSCINT00000035165 | TAGCCGCCACACATGTAA    | GCAGCAAGAGCTGCATCAT   |



|                             |                                |                    |                      |                       |
|-----------------------------|--------------------------------|--------------------|----------------------|-----------------------|
| Collagen, type XIV, alpha 1 | VWF domain containing protein  | ENSCINT00000036027 | CGATCGCTCACGTAACAAAC | TTCCTGCAGTGTGTAGGCTCT |
| EMX                         | EMX Homeobox                   | ENSCINT00000037147 | CCACCAGGATTCCAACAAAC | TCAGCTCCAACCACGTAATG  |
| IGFbp                       | MAC25-like                     | ENSCINT00000037260 | TTCATTTGGTAGGTGCGTGA | TATTCACACGATGCGGAAGA  |
| Villin-1                    | Villin-1                       | ENSCINT00000003800 |                      |                       |
| SFI1-like                   | SFI1-like                      | ENSCINT00000008827 |                      |                       |
| Sideroflexin-1-like         | Sideroflexin-1-like            | ENSCINT00000010013 |                      |                       |
| NEK7-like                   | NIMA related kinase 7-like     | ENSCINT00000017101 |                      |                       |
| Ubiquilin-1                 | Ubiquilin-1                    | ENSCINT00000017880 |                      |                       |
| MYBB1A                      | MYB Binding 1A                 | ENSCINT00000018013 |                      |                       |
| LIMK1-like                  | LIM Kinase 1 Like              | ENSCINT00000024269 |                      |                       |
| Myosin X                    | PH domain containing protein   | ENSCINT00000033884 |                      |                       |
| Kinesin                     | Kinesin                        | ENSCINT00000035420 |                      |                       |
| LMNTD1                      | Lamin tail domain containing 1 | ENSCINT00000036416 |                      |                       |

**Table S6. Analysis of Variance (ANOVA) Results for qRTPCR.** The columns indicate the type of gene product that was tested (either microRNA or mRNA); the name of the gene product; intermediate statistics used for ANOVA calculation (sum of squares, mean of squares, F value), p-value and the final column indicates level of significance ('\*\*\*'  $\leq 0.001$ , '\*\*'  $\leq 0.01$ , '\*'  $\leq 0.05$ ).

| Type  | Name        | Df | Sum Sq | Mean Sq | F-value | P-value  | Sig |
|-------|-------------|----|--------|---------|---------|----------|-----|
| mRNA  | bZip        | 3  | 369.7  | 123.23  | 76.21   | 6.52E-09 | *** |
| mRNA  | Caspase2    | 3  | 37.76  | 12.59   | 0.85    | 0.485    |     |
| mRNA  | DIAP2       | 3  | 30.14  | 10.047  | 1.011   | 0.412    |     |
| mRNA  | Hlx         | 3  | 76.36  | 25.453  | 4.955   | 0.0138   | *   |
| mRNA  | HSP70       | 3  | 35.92  | 11.973  | 2.16    | 0.135    |     |
| mRNA  | IGF-like    | 3  | 33.39  | 11.13   | 7.233   | 0.00363  | **  |
| mRNA  | IGFbp       | 3  | 159.48 | 53.16   | 10.51   | 0.000699 | *** |
| mRNA  | NEK11-like  | 3  | 47.02  | 15.674  | 4.067   | 0.0166   | *   |
| mRNA  | Prospero    | 3  | 11.46  | 3.819   | 0.714   | 0.559    |     |
| mRNA  | Rev-erb     | 3  | 66.35  | 22.116  | 9.767   | 0.00122  | **  |
| mRNA  | TLR         | 3  | 53.01  | 17.67   | 2.714   | 0.0587   | .   |
| mRNA  | TNFR        | 3  | 122.2  | 40.73   | 363     | 6.94E-09 | *** |
| mRNA  | TNFR-assoc  | 3  | 6.24   | 2.08    | 0.299   | 0.825    |     |
| mRNA  | Tolloid     | 3  | 177.5  | 59.18   | 6.677   | 0.00138  | **  |
| mRNA  | Tomoregulin | 3  | 157.4  | 52.48   | 13.32   | 2.55E-06 | *** |
| miRNA | miR-1-3p    | 3  | 0.0407 | 0.01355 | 0.166   | 0.918    |     |
| miRNA | miR-125-5p  | 3  | 0.057  | 0.01916 | 0.15    | 0.929    |     |
| miRNA | miR-126     | 3  | 1.401  | 0.4671  | 3.01    | 0.0445   |     |
| miRNA | miR-133c    | 3  | 0.0321 | 0.01069 | 0.67    | 0.577    |     |
| miRNA | miR-217     | 3  | 2.476  | 0.8255  | 2.209   | 0.108    |     |
| miRNA | miR-219     | 3  | 6.221  | 2.0737  | 658.3   | 6.51E-10 | *** |
| miRNA | miR-29      | 3  | 12.213 | 4.071   | 283.7   | 1.84E-08 | *** |
| miRNA | miR-31      | 3  | 1.195  | 0.3982  | 2.31    | 0.095    |     |
| miRNA | miR-3598-5p | 3  | 0.602  | 0.2007  | 0.746   | 0.533    |     |
| miRNA | miR-4009c   | 3  | 0.9938 | 0.3313  | 81.52   | 2.45E-06 | *** |
| miRNA | miR-4030-5p | 3  | 2.742  | 0.9141  | 1.133   | 0.351    |     |
| miRNA | miR-4036-5p | 3  | 0.8846 | 0.29485 | 4.613   | 0.0138   | *   |
| miRNA | miR-4043-5p | 3  | 2.174  | 0.7248  | 3.356   | 0.0323   | *   |
| miRNA | miR-4053-3p | 3  | 0.6399 | 0.2133  | 3.224   | 0.037    | *   |
| miRNA | miR-4065-3p | 3  | 0.3767 | 0.12558 | 140.7   | 2.92E-07 | *** |
| miRNA | miR-4065-5p | 3  | 0.4692 | 0.1564  | 10.41   | 0.00389  | **  |
| miRNA | miR-9-5p    | 3  | 5.023  | 1.674   | 1.593   | 0.275    |     |

**Table S7. microRNA Alignment Summary.** This is the summary output reported by miRDeep2 for all miRNA samples. The upper section summarizes the number of and confidence in novel microRNAs identified by miRDeep2 from our samples. The lower three sections detail the number of reads, sequences and putative homology for all microRNAs detected by miRDeep2.

[Click here to Download Table S7](#)

**Table S8. Transcript Mappings to Functional Categories.** The membership of each transcript in corresponding functional categories is listed here. The first column is the description of the functional category; the second column is the Ensembl transcript identifier of a transcript belonging to that category; the third column is the unique identifier for the category.

[Click here to Download Table S8](#)

**Table S9. Time series Z-scores.** The z-scores of each functional category during regeneration are listed here. Z-scores for each category were calculated from the mean  $-\log_2$  FDR estimated by DESeq2 and EdgeR for each transcript relative to one of the two chosen reference stages (D0 and NR). The first column designates the overarching type of classification for each category; the second column gives the description of the functional category; subsequent columns list z-scores for each comparison of stages. Each comparison is indicated by the reference stage symbol followed by a dash then the symbol for the relative stage of regeneration. Reference stage symbols are: NR = Non-regenerating, D0 = zero days post-amputation (dpa). Regeneration stage symbols are: D1 = one dpa, D3 = three dpa, D8 = eight dpa.

[Click here to Download Table S9](#)

**Table S10. Correlation Network.** microRNA-target interactions predicted by TargetScanS that are supported by Pearson correlation ( $\rho \leq -0.9$ ) of the mean  $\log_2$  fold-change estimated by EdgeR and DESeq2 at each stage relative to zero days post-amputation (D0). Each included microRNA-target pair is only listed once even if it had more than one predicted binding site for a given target. The first column designates the Ensembl transcript identifier; the second column designates the microRNA name; the third column indicates the correlation between expression levels.

[Click here to Download Table S10](#)

**Table S11. Network Clusters.** microRNA-target clusters predicted by the Moduland plugin for Cytoscape. The first column contains either the microRNA name or target transcript Ensembl identifier; the second column contains the name of the cluster corresponding to the node in column 1, which is the name of the node determined to be the most important node in that cluster.

[Click here to Download Table S11](#)

**Table S12. Network Cluster Functional Enrichments.** microRNA targets in a given network cluster that significantly overlap ( $FDR \leq 0.05$ ) with transcripts in a given functional category determined by a hypergeometric test are shown here. The first column designates the overarching type of classification for each category; the second column gives the description of the functional category; the third column gives the name of the network cluster; subsequent columns indicate the number of transcripts in the network cluster, number of transcripts in the functional category, number of transcripts overlapping between the two lists, p-value and false discovery rate (FDR) adjusted p-values. P-values are the probability of at least the specified number of transcripts overlapping between the two lists as determined by a hypergeometric test for enrichment.

[Click here to Download Table S12](#)